Title
Cross-Species Mechanisms of Orientation Tuning in the Primary Visual Cortex

Author
Jimenez, Luis

Publication Date
2021

Peer reviewed|Thesis/dissertation

UNIVERSITY OF CALIFORNIA

Los Angeles

Cross-Species Mechanisms of Orientation Tuning in the Primary Visual Cortex

A dissertation submitted in partial satisfaction of the requirements

for the degree of Doctor of Philosophy in Psychology

by

Luis Jimenez

2021

ABSTRACT OF DISSERTATION

Cross-Species Mechanisms of Orientation Tuning in the Primary Visual Cortex

by

Luis Jimenez

Doctor of Philosophy in Psychology

University of California, Los Angeles, 2021

Professor Dario L. Ringach, Chair

Simple cells in the primary visual cortex of all mammals are renown for having an ‘orientation preference’, meaning that they respond to a specific orientation of an elongated stimulus that lands on their spatial receptive field. Moreover, these cells respond to increments and decrements in luminance in slightly separate regions of their receptive fields, and the angle formed by the centers of these regions can predict their preferred orientation. Despite decades of research into the topic, the mechanism that gives rise to tuned simple cells and their receptive field structure remains an open question. Many models struggle to explain why the properties of simple cells are similar across mammals despite substantial inter-species differences in how simple cells are spatially organized across the cortex. For instance, in the primary visual cortex of cats and primates, vertical columns of cells have similar orientation preferences, and the preferences of

these columns rotates smoothly, in a quasiperiodic fashion, as one moves horizontally across the cortex. In contrast, simple cells in mouse primary visual cortex with different tuning preferences are scattered randomly throughout the cortical tissue. Here I assess a mechanistic model of tuning asserting that a single mechanism can generate tuned cells that are either mapped out in an orderly manner across the cortex or arranged in a salt and pepper fashion. The two projects carried out in this thesis test a specific prediction made by the model and compare it to physiological data in mouse primary visual cortex and the thalamic afferents that innervate the cortex. Overall, the results corroborate the model and lend support to the notion that a universal, cross-species mechanism may be used to encode the orientation of a visual stimulus.

The dissertation of Luis Jimenez is approved.

Zili Liu

Hongjing Lu

Tad Blair

Dario L. Ringach, Committee Chair

University of California, Los Angeles

2021

TABLE OF CONTENTS

LIST OF FIGURES

LIST OF ABBREVIATIONS

Cpd: cycles per degree of visual space

dLGN: Dorsal lateral geniculate nucleus

L1: Layer 1 of primary visual cortex

L2/3: Layers 2 and 3 of primary visual cortex

L4: Layer 4 of primary visual cortex

L5: Layer 5 of primary visual cortex

L6: Layer 6 of primary visual cortex

RGC(s): Retinal Ganglion Cell(s)

RF(s): Spatial Receptive field(s)

SC: Superior colliculus

V1: Primary Visual Cortex

VITA

EDUCATION

University of California, Los Angeles

PhD candidate in Psychology and Behavioral Neuroscience

Los Angeles, Ca; Sep 2016 – Jun 2021

- 2018 UCLA Graduate Summer Research Mentorship Program Award
- 2018 American Physiological Society APS select award
- 2018 Honorable Mention for NSF Graduate Research Fellowship
- 2016 UCLA Eugene V. Cota-Robles Fellow
- 2016 UCLA Competitive Edge Scholar

University of California, Los Angeles

Bachelor's in Psychology and Cognitive Science

Los Angeles, Ca; 2012 – 2014

- 2013 UCLA Psychology Research Opportunities Program Scholar

RESEARCH

University of California, Los Angeles

Graduate Researcher Los Angeles, Ca

Sep. 2016 – Present

- Advisor: Dario L. Ringach

TEACHING

University of California, Los Angeles

Teaching Fellow for Undergraduate Courses in Neuroscience and Psychology

Los Angeles, Ca; Summer 2017, Sep. 2021 – Aug 2021

University of California, Los Angeles

Teaching Fellow: Graduate Level Courses in Statistics

Los Angeles, Ca; Sep. 2017 – Jun 2018, Sep. 2019 – Jan. 2020

OUTREACH

SACNAS, UCLA Chapter

Outreach and Social Media Coordinator

Los Angeles, Ca; Oct 2017 – May 2019

PUBLICATIONS AND PREPRINTS

Publications

- Jimenez, L. O., Tring, E., Trachtenberg, J. T., & Ringach, D. L. (2018) Local tuning biases in mouse primary visual cortex. Journal of Neurophysiology. https://doi.org/10.1152/jn.00150.2018

- Silva, A. E., Barakat, B. K., Jimenez, L. O., & Shams, L. (2017). Multisensory congruency enhances explicit awareness in a sequence learning task. Multisensory Research. doi: 10.1163/22134808-00002587.

Preprints

- Jimenez, L. O., Tring, E., Trachtenberg, J. T., & Ringach, D. L. (2017). Untangling cortical maps in mouse primary visual cortex. bioRxiv. https://doi.org/10.1101/102079 - preprint (http:// biorxiv.org/content/early/2017/01/21/102079.abstract)

PRESENTATIONS

- Jimenez, L. O., Tring, E., Trachtenberg, J. T., & Ringach, D. L. (2018) Poster, Local tuning biases in mouse primary visual cortex. Journal of Neurophysiology. https://doi.org/10.1152/jn.00150.2018
- Local tuning biases in mouse primary visual cortex. Poster, Dynamics of Neural Microcircuits Symposium, University of California, Los Angeles (May 2018)
- Synaptic organization of visual space in primary visual cortex. Presentation, Department of Psychology, University of California, Los Angeles (January 2018).
- Untangling cortical maps in mouse primary visual cortex. Poster, Society for Neuroscience, Washington D.C. (November 2017)
- Topology of ON and OFF inputs in visual cortex enables an invariant columnar architecture. Presentation, Department of Psychology, University of California, Los Angeles (January 2017).
- Paik, S. B. & Ringach, D. L. Retinal Origin of Orientation Maps in Visual Cortex. Presentation, Competitive Edge Program Seminar, University of California, Los Angeles (August 2016)
- Visual Rhythm Perception Improves Through Auditory but Not Visual Training. Presentation, Psychology Research Opportunities Program Scholar Research Seminar, University of California, Los Angeles (June 2014)

OTHER SKILLS

- Computer: MATLAB, Python, R, SPSS, STATA, Processing, Arduino, Swift
- Languages: Proficient in English and Spanish

PROFESSIONAL ACTIVITIES

Society for Neuroscience (SFN) 2017–present

Society for the advancement of Chicanos and Latinos in Science (SACNAS) 2017–present

Overview

Mammals are visual beings. Their vision helps them detect predators, identify prey or mating partners, and navigate their environment. A key step to understanding how vision works is to study how the visual systems of different species process images that strike the eye. Images contain a vast amount of information but neurons in the early visual system of all mammals selectively respond to a few important features, most notably, the location, contrast polarity (increase or decrease in luminance) and the orientation of stimulus parts.

How do visual neurons work together to encode these image features, specifically, what allows neurons to encode the orientation of a stimulus? Is there a universal process used by the visual system of all mammals to encode the orientation of a stimulus? Or do different mammals - which have different behavioral needs, that live in different environments, and that perform different visual tasks – process images in a different manner? These are the two general questions that this thesis aims to answer.

THE EARLY VISUAL SYSTEM OF THE MOUSE

EYES + RETINAL GANGLION CELLS

The mouse is a small nocturnal mammal that views the world from near the ground. Its eyes are located on the sides of its head, offering it an extensive view of its surrounding environment (up to 320 degrees wide) but limiting its binocular view of the frontal visual field (40 degrees wide) [1-3] (**Figure 1**).

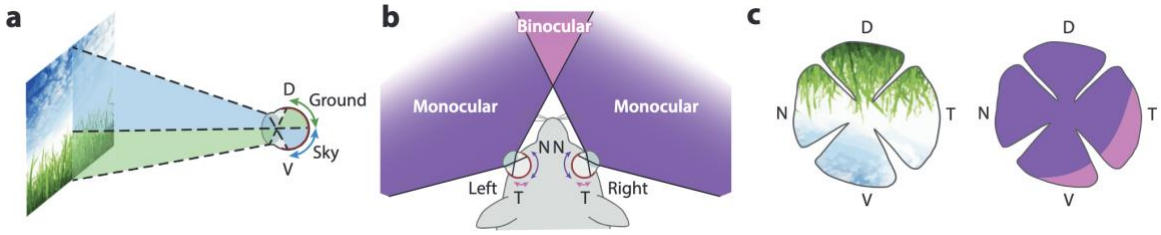

FIGURE 1 VISUAL SPACE OF THE MOUSE

(A) *Images from the upper and lower part of visual space project onto the ventral and dorsal regions of the mouse retina, respectively.* ***(B)*** *The central region of visual space projects onto the temporal retinas of both eyes, while images from the lateral environment project onto the nasal retinas.* ***(C, left)*** *Example of an image of the mouse's environment projecting onto its retina.* ***(C, right)*** *Illustration of the retinal regions receiving information from the central visual field (pink regions) and the lateral visual field (dark purple regions); Figure adapted from Heukamp 2020*

SAMPLING THE IMAGE

Images from the environment are projected onto the retina which can be subdivided into 5 layers [4]. The inner most layer contains the array of photoreceptors that transduce light into an array of neural signals. This array of signals is passed onto the horizontal cell layer, bipolar cell layer, amacrine cell layer, and finally, the layer of the ganglion cell [5]. In mice, at least thirty different retinal ganglion cells (RGCs) are believed to exist [6-9], with possibly more cell types that have yet

to be discovered [6]. In this thesis I focus on a specific set of mouse RGCs that choose to respond to the contrast polarity and motion direction of stimuli presented within their spatial receptive fields.

Mosaics of regularly spaced RGCs

The spacing between the cell bodies of RGCs of the same type is highly regular in both mice [6] and other mammals [8,10,11]. This regular spacing essentially creates a mosaic of cell bodies that tile the retinal surface. Many different mosaics exist, each composed of a unique type of RGC with its own unique spacing [8,10,12], allowing every type of RGC to independently sample the visual image at different spatial resolutions.

RGC coverage of image regions

The *coverage factor* of an RGC refers to the number of times its RF covers, or samples, a given a point of the visual image. Although some RGCs show larger spacing between their cell bodies than others, nearly all mouse RGCs sample each point in the retina about two to three times [6] . For example, stimulus motion presented within a point in visual space can lead to a population response of four subtypes direction selective RGCs each tuned to one of the four cardinal directions.

The mouse retina, however, is unique in that certain RGCs can vary their coverage depending on their general retinal location. Center-surround RGCs show greater coverage of the temporal retina compared to the nasal areas [13,14] The retina is also non-uniformly covered by W3-RGCs, which densely cover ventral regions but show sparser coverage in the dorsal and peripheral regions [14]. Interestingly, the density of ON-center RGCs in the retina seems to increase along a nasal-temporal gradient [13]. The progressive increase in the density of these RGCs occurs in the ventral-temporal retina, which receives the images from frontal visual field (**Figure 1)**.

SPATIAL RECEPTIVE FIELDS OF RGCS

The most defining feature any visual neuron is its spatial receptive field (RF), which refers to the region of visual space (i.e., region of the retina) a stimulus must be in to elicit a response in the neuron. The RFs of retinal cells are primarily determined by their position in the retina and the spatial layout of their dendritic arbors [8,15]. RGCs that project to the dLGN have RFs that range from about 5 degrees to about 10 degrees of visual space in diameter. For example, *F-RGCs* have RFs that extend ~4 degrees of visual space, ON/OFF direction selective RGCs extend ~7 degrees, and center-surround RGCs have RFs extending ~6 to 11 degrees [6,16,17] **(Figure 2).** As a reference, it would take about 35 center surround RGCs to completely tile the 320 degree wide horizontal visual field of the mouse **(Figure 1**).

CONTRAST POLARITY TUNING

RGCs are *tuned,* or *selective,* to specific features of a stimulus that lands on their RFs [8,13]. Center surround RGCs, for example, are tuned to polarity; that is, they are selective to the spatial and temporal contrast of a stimulus (i.e., changes in luminance across space and time). ON center-surround RGCs respond best to a stimulus that increases in luminance (e.g., the appearance of a *bright spot* one a dark background), while OFF center RGCs respond best to

luminance decrements (e.g., the appearance of a *dark spot* on a bright background) [6,18]. These center surround cells come in two flavors: those with sustained temporal response, and those with transient responses [19]. Polarity tuned RGCs are found in the retinas of all mammals [20].

DIRECTION TUNING

A separate class of RGCs, known as ON/OFF direction-selective RGCs, respond robustly to stimuli that sweep across their RF along one of the four cardinal directions [21] **(Figure 2)**. Direction tuned RGCs have various RF sizes and various preferences to the speed of the stimulus movement. Most of these direction tuned RGCs have a preference for *both* dark and bright stimuli (e.g., they respond to the leading or trailing edge of a dark motion stimulus) [6]. A more recently discovered cell type is the *W3-RGC* which has a small RF and responds only when a dark object moves, regardless of its direction [22].

VARIATIONS IN TUNING ACROSS THE RETINA

Some of RGCs change their tuning depending on their general location in the retina. When center-surround RGCs in the ventral retina are stimulated, their response is short, while those in the dorsal retina have more sustained responses [14,23]. J-RGCs respond well to dark upward-moving stimuli when located on the central horizontal meridian of the retina but are less selective to direction when located in the dorsal and ventral retinal regions [14,24]. Furthermore, various types of RGCs in the dorsal retina are highly sensitive to green but not UV light, whereas those in the ventral retina prefer UV light [14,25-28].

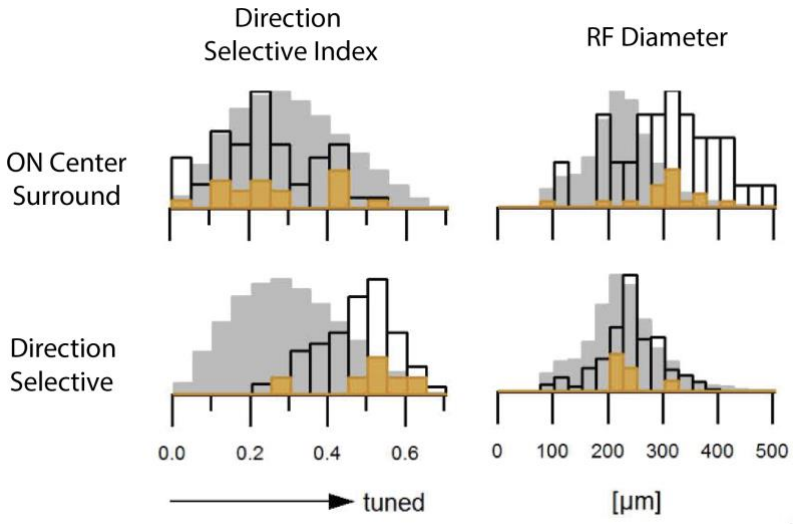

FIGURE 2 SPATIAL SIZE AND TUNING OF CENTER SURROUND AND DIRECTION SELECTIVE RGCS.

Gray distributions describe the direction selectivity (left distributions) and RF diameter (right distributions) of an entire population of ~8000 RGCs, classified into 32 different functional types by Baden 2016. White distributions describe the direction selectivity and RF diameter a population of RGCs classified as ON center-surround RGCs (Top Row) and ON-OFF direction selective (Bottom Row). In text, diameter of RGCs in micrometer units are converted to degrees of visual space by assuming 31 degrees per micrometer (Remtulla 1985)

RETINOTHALAMIC NETWORK

In mice, only about 10% of all RGCs project to the dorsal lateral geniculate nucleus (dLGN)[18,29,30], while the majority project to the superior colliculus (SC) [31,32]. This runs in contrast to other mammals (e.g., primates), where the majority of RGCs project to the thalamus [2]. Nevertheless, at least 75% of all known functional types of RGC types innervate the dLGN [21,33].

CONTRALATERAL AND EYE SPECIFIC PROJECTIONS

In mice, each retina receives images that, for the most part, originate from the lateral portion of the environment **(Figure 1)**. Most RGC axons from each eye project across the optic chiasm so that visual signals from the lateral environment of the mouse are relayed onto the contralateral side of the brain.

RGCs from all regions of the retina project axons that terminate throughout the contralateral dLGN [30,34] **(Figure 3)**. However, some RGCs originating from a small area of the ipsilateral ventral retina (which receives images from the central, binocular, visual field) send afferents to a small cylindrical region of the dLGN [30] **(Figure 3).**

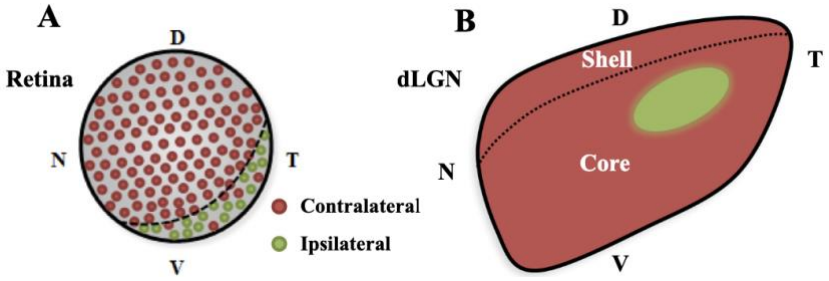

FIGURE 3 ORIGIN AND THE TARGET REGION OF RETINO-THALAMIC AFFERENTS

(A) *The contralateral dLGN receives input from RGCs residing in all regions of the retina (red circles). The majority, but not all, RGCs in a small crescent region of the ventral-temporal region (green circles, below the dashed line) send their afferents ipsilaterally.* ***(B)*** *RGC afferents from the contralateral eye innervate all areas of the dLGN (red area), while those from the ipsilateral eye are sent to the central region near the core (green). N, nasal; T, temporal; D, dorsal; V, ventral; Figure taken from Guido 2018*

SPACE

The spatial relationships between the axons of RGCs are maintained as they project from the retina to the dLGN [33-36]. Thus, the afferents of RGC with similar spatial RFs innervate similar areas of the dLGN [21,30,37] , which create a retinotopic map of inputs to the thalamus **(Figure 4)**.

At a fine spatial scale, this retinotopic order of RGC inputs is lost: the RF locations of neighboring RGC boutons randomly scatter by ~2 degrees of visual space [33] **(Figure 4)**. Therefore, the dLGN receives a retinotopically ordered set of signals, but only on a coarse spatial scale.

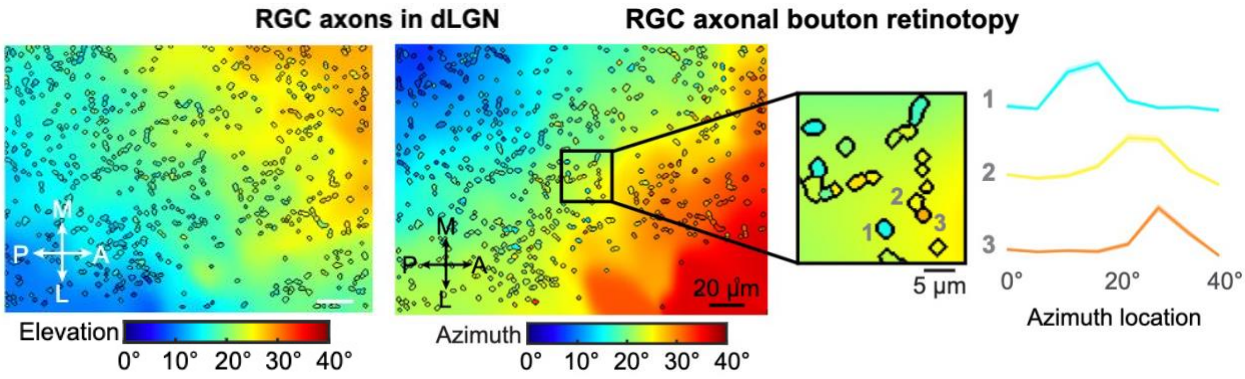

FIGURE 4 RETINOTOPIC ORDER OF RGC BOUTONS INNERVATING THE DLGN.

(LEFT, MIDDLE) *Orderly retinotopic organization of elevation (left) and azimuth (middle) of RGC axons innervating the dLGN of an example mouse.* ***(MIDDLE INSET, RIGHT)****. Zooming in reveals a scatter of retinotopic preference among neighboring boutons; Figure adapted from Liang 2018*

CONTRAST POLARITY AND DIRECTION TUNING

The mouse retina contains center-surround RGCs that respond best to either the onset or offset of a circular stimulus and can have sustained or transient temporal responses [6,7,17,19]. The axonal afferents of these center-surround RGCs targeting the dLGN are relatively large [34], and innervate all regions of the dLGN, especially the medial part of the dLGN, known as the *core* [29,38,39] (**Figure 5**).

The dLGN, especially the outer region known as the *shell*, also receives inputs from at least three distinct classes of RGCs selective to a specific direction of a moving stimulus [29,39] **(Figure 5).** These include the posterior direction preferring ON-OFF RGC [39-42], the J-RGC with an upward direction preference and exclusively an OFF response [24,29,39,43], and the F-mini RGC known for its small spatial RF [17,29]. Compared to the axonal arbors of center-surround RGCs, those of some direction-selective RGCs may be narrower [34].

LATERAL GENICULATE NUCLEUS

OCULAR DOMINANCE AND SPATIAL TUNING

Since most RGC axonal projections cross the optic chiasm, most dLGN neurons acquire an exclusive response to stimuli that fall onto the contralateral eye [30]. However, anatomical [44] and functional [45] studies show that some dLGN neurons are targeted by RGCs in the ipsilateral retina as well.

The diameter of the RFs of dLGN neurons range from about 10-20 degrees wide [34,46,47]. This spatial size is slightly larger than those of center-surround and direction selective cells in the retina [17] **(Figure 2),** and also similar to the RF size of RGC boutons that innervate the dLGN [33] **(Figure 4, see inset).**

In addition, dLGN neurons are retinotopically organized [34] in a manner that, not surprisingly, matches the retinotopic arrangement of the RGC afferents that target the dLGN [33] **(Figure 4).** Specifically, the nasal to temporal visual region is mapped along the medial to lateral axis of the dLGN, while the upper to lower visual field is lies across the dorsal to ventral axis of the dLGN [30,33,34].

CONTRAST POLARITY

Neurons in the dLGN have ON or OFF center-surround RFs [34,45,47,48], much like those in the retina. Center surround cells make up the majority of cells in dLGN [30,34,45-48], although they are a minority (~5%) in the retina suggesting that the vast majority of dLGN inputs come from these center-surround RGCs [34]. The dLGN core region, in particular, houses a large proportion of these center-surround cells [34,39,48] **(Figure 5)**.

The RFs of center surround dLGN cells have circular central subregions [34,46,47] that, generally, are surrounded by an annulus with an opposite preference for contrast polarity [34,48]. Stimulation of their central subregion can elicit a sustained, transient, monophasic [34], or biphasic [34,48,49] temporal response. Moreover, these center-surround dLGN cells are *not* selective to the direction of a stimulus moving across their RF [34,47,48]. Many the spatial and temporal response properties of center-surround dLGN neurons are similar to those of center surround RGCs.

ORIENTATION (AXIS/DIRECTION) TUNING

According to a classical view, the thalamus is said to lack cells that are tuned to stimulus orientation [21,50,51]. In mice this is not the case. Some neurons in the dLGN, especially those in the shell region **(Figure 5**), are clearly orientation tuned [9,33,34,39,48,52].

Two types of orientation tuned cells are found in the mouse dLGN. *Direction*-selective cells respond to a stimulus moving in only one particular direction (e.g., the upward movement only) with weaker responses to motion in the opposite, null direction (similar to those in the mouse retina [6]), while *axis*-selective cells respond best to both motion directions that form a particular axis (e.g., both upward *and* downward movement) [9,33,34,39,45,46,48,53,54]. Unless specified, I refer to both *direction* and *axis* tuned cells as *orientation* tuned neurons.

Evidence for axis-selective cells is relatively scarce in the mouse retina [21] (but see reference [6]), nor is known if they project to the dLGN [21] (but see reference [33]). *Axis* selective neurons in the dLGN appear to be more numerous and have sharper tuning than *direction* tuned neurons [9,33,34,45,55] (but see reference [46] for alternative findings). Most orientation selective dLGN neurons tend to prefer cardinal directions or axes of motion [9,33,34,53,54], similar to direction tuned RGCs. In two studies specifically, tuned dLGN neurons were biased towards motion in the vertical direction [45,54].

The spatial structure of the RFs of orientation tuned neurons in the dLGN vary in size and shape: They can be circular, elongated, have multiple peaks, or have no discernable structure [34,45,46,48,56]. In some studies, the elongated structure of direction tuned RFs predicted their orientation preference, although with considerable error overall [46,48,56]. Unlike center-surround dLGN neurons (with exclusively ON or OFF-center responses) orientation-tuned neurons tend to be evoked by motion stimuli of both contrasts (both the onset *and* offset)[34,46,48], which is also similar to many direction selection RGCs.

DLGN SHELL VS. CORE

Striking differences exist in both the inputs and outputs of neurons in the shell versus the core region of the mouse dLGN (Figure 5). For example, the shell of the dLGN is targeted by several types of direction-selective retinal cells, while the core receives many projections from the center-surround RGCs that are not tuned to orientation [39] . Compared to the core, the shell region tends to be innervated with clusters of boutons from different types of retinal cells [57,58], suggesting the shell is driven by a more diverse set of retinal signals [33]. The shell is heavily populated with neurons tuned to orientation, whereas those in the core are non-selective and have center-surround RFs [30,34,39,48,53]. The shell region also contains neurons that morphologically resemble W-like cells in cats, while the core is populated by cells that resemble the X and Y cells in cats [30]. Shell neurons send their outputs to neurons in the superficial layers of the primary visual cortex (V1), while neurons in the core appear to preferentially target V1 neurons in layer 4[39] (see next section). In summary, the neurons in the shell and the core receive different RGC inputs, differ in their tuning to stimulus features, and target different layers in V1. These observations suggest that two separate streams of visual information - polarity and motion - flow through the shell and the core of the mouse dLGN.

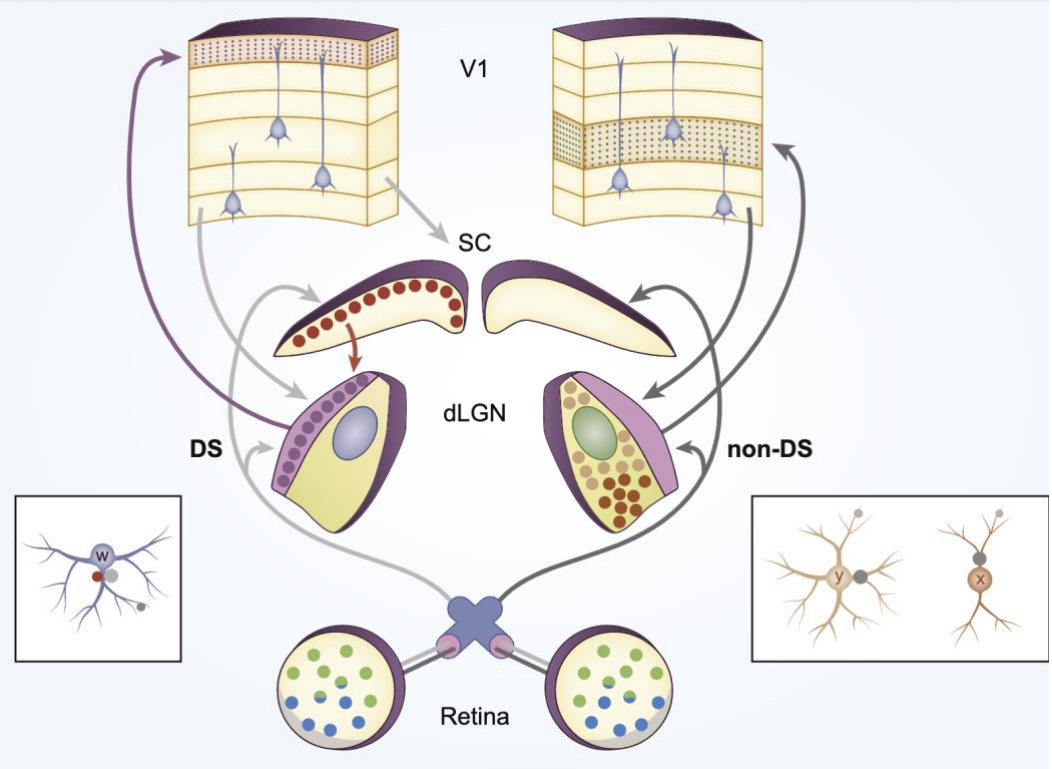

FIGURE 5 PARALLEL VISUAL PATHWAYS IN THE MOUSE'S EARLY VISUAL SYSTEM

(LEFT HEMISPHERE) *The left hemisphere illustrates the putative 'orientation tuned' pathway. Afferents of direction tuned RGCs project mainly to the outer shell of the dLGN, where a large proportion of cells show orientation tuned responses and W-cell-like morphological properties. dLGN neurons in the shell project to the superficial regions of the primary visual cortex where the apical dendrites of L2/3 cells reside.*

(RIGHT HEMISPHERE) *The right hemisphere illustrates an example of the 'untuned' selective visual pathway. Afferents of non-direction selective RGCs (e.g., center-surround RGCs) project mainly to the inner dLGN core region heavily populated with center-surround neurons with X/Y cell-like morphologies. dLGN neurons in the core send their outputs to L4 of the primary visual cortex.*

(NOTE) *Note that most RGCs send projections to the contralateral dLGN, but a small proportion (cells in the gray region of the retina) project ipsilaterally to a small region (the egg-shaped region in dLGN) within the core. The blue to green gradient running from the ventral to dorsal retina corresponds to the variation of RGC stimulus selectivity (e.g., variations in selectivity to UV vs. green light) across the mouse retina.*

Figure adapted from Busse 2018

THALAMOCORTICAL NETWORK

LAYER SPECIFIC PROJECTIONS OF DLGN

Of all subcortical structures, the thalamus provides the majority of the input to the primary visual cortex (V1) [59]. In mice, the density of thalamic axon patches targeting V1 is estimated to be 5000 axons/mm^2, which is relatively larger than that observed other species [32].

Mouse V1 can be subdivided into 5 to 6 layers. dLGN axons synapse onto all layers of mouse V1, but most densely target V1 cells layer 4 (L4)[39,54,60-62] . The deeper portion of layers 2/3 (L2/3) and layer 5 (L5) of V1 receive less, yet still substantial, input from the dLGN [39,60-62].

The superficial layers of the cortex (i.e., Layer 1 (L1) and upper L2/3) are preferentially targeted by afferents of neurons in the outer shell region of the dLGN, **(Figure 5**), and extracortical regions as well [63]. Interestingly, dLGN axon terminals form periodically arranged clusters across surface of L1 [63]. L4 is preferentially innervated by axons from the inner core of the dLGN [39] **(Figure 5)**, although other layers also receive inputs from the core [54].

Given that L4 is the primary target layer of the dLGN, L4 cells are highly sensitive when the dLGN is directly stimulated [61,62]. It is estimated that approximately one-third of the total excitatory input reaching cells in L4 comes from the dLGN [64,65], a fraction that is slightly smaller to estimates in the cat [66,67] . L2/3 neurons in mice are also highly responsive to direct stimulation of the dLGN, especially those in lower L2/3 who respond to dLGN input in a way that matches and sometimes exceeds those of L4 neurons [61,62].

ORIENTATION AND POLARITY TUNING

Both direction selective [39] and ON/OFF center [39,49,65] dLGN neurons innervate mouse V1. The dLGN core, which populated by center surround cells, appears to preferentially target V1 neurons in layer 4[39], while the direction tuned shell region of the dLGN sends its axons to the superficial layers V1 [39] (although this dichotomy is not absolute [54]). Tuned dLGN neurons [9,33,34,45,48,53] and their axonal projections to V1 [39,54] also show a biased preferences towards cardinal orientations [54,68].

PRIMARY VISUAL CORTEX

LOCAL NETWORKS OF V1 NEURONS

Neurons in V1 receive local, intracortical inputs (i.e., they are driven by other cells within V1). L2/3 neurons receive a large number of *excitatory* inputs from cells residing below them in L4 [69,70] and, to a lesser extent, from cells in L5 [60,69-71] and horizontally positioned L2/3 cells [60,69-73] **(Figure 6)** . Moreover, connected groups of excitatory cells in L2/3 tend to be driven by the same excitatory L4 cell [71]. Only about a third of all inputs to L2/3 cells come from other V1 *inhibitory* cells [69,70], however, inhibitory inputs between L2/3 cells [69,70] are stronger than excitatory inputs between them [60]. L2/3 cells also receive inhibitory input from deeper cells in L4 [71]. Within L4, excitatory cells make strong excitatory horizontal (lateral) connections with each other [62,64,65], and weaker horizontal inhibitory connections also exist [60,64,65]. Interestingly, pairs of connect L4 and L2/3 cells, are both targeted by the same dLGN afferent [62].

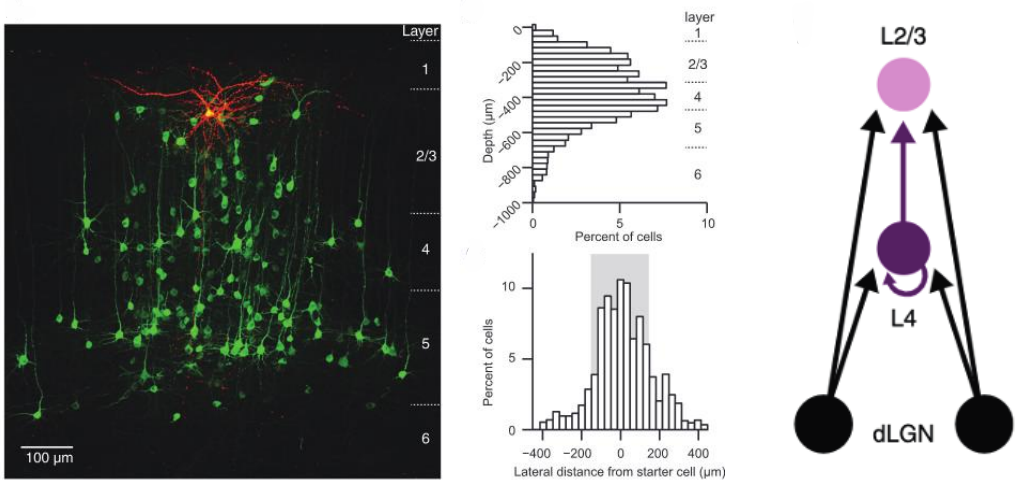

FIGURE 6 LOCAL NETWORKS IN MOUSE V1

*(**LEFT**) Confocal image of an electroporated L2/3 excitatory neuron (red cell) and the network of presynaptic cells connected to it (green cells). Presynaptic cells consist of mostly excitatory neurons (vs. inhibitory).*
*(**MIDDLE**) Distribution of depth distances (top) and lateral distances (bottom) between a L2/3 neuron and cells in its presynaptic network. The majority of inputs to a L2/3 starter cell originate from L4.*
*(**RIGHT**) Pairs of trans-laminarly connected cells (L4→L23) receive the same dLGN input, and horizontally connected L4 cell pairs (L4←→L4) receive the same dLGN inputs*
Left and middle Figure taken from Wertz 2015. Far right figure taken from Morgenstern 2016.

NETWORKS OF CELLS SHARE TUNING AND LINEAGE

Excitatory networks of connected cells tend to have similar visually driven behavior. L2/3 networks are composed of cells with correlated activity (in response to 'naturalistic' stimuli)[72-74], are driven by regions of visual space [74], and have similar orientation preferences [69,72,73]. In L4, connected excitatory neurons modulate at the same phases in response to sinusoidal input [65]. Interestingly, these networks of neurons with similar preferences in mouse V1 resemble those of other mammals where V1 domains of similar orientation preferences are connected [75-77].

However, the biases in the responses among connected cells in mouse V1 are not absolute, as many cells with different tuning preferences can also be connected [60].

In the adult mouse cortex, sibling neurons - clonally related cells born out of the same progenitor cell - are preferentially connected [78]. These siblings also tend to have matching orientation preferences [68]. The formation of these 'sibling networks' is believed to be caused by the gap junctions that sibling neurons share early in development [79,80]. These gap junctions endow siblings with overlapping spatial RFs [73] at eye-opening, allowing their activity to be correlated throughout development, ultimately giving rise to chemical synapses [80], and similar preferences to stimulus orientation [79].

SPACE

LAYER SPECIFIC SIZE AND SHAPE OF V1 SPATIAL RFS

Not surprisingly, mouse V1 contains cells that are tuned to the spatial location of a visual stimulus [52,81,82]. The sizes of the spatial RFs of mouse L2/3 and L4 excitatory cells range from ~6 to ~15 degrees wide [63,73,81-87], and their spatial shape is more asymmetric than cells in deeper layers [63]. Inhibitory neurons across all layers and excitatory cells in L5 tend to have larger RF sizes than excitatory neurons in L2/3 and L4 [63,81,83,85] **(Figure 7).** Interestingly, V1 neurons in mouse [73,81,82] and primate [88] have spatial RFs with strikingly similar asymmetric structures (see [81] for direct comparison).

The spatial resolution of V1 neurons can also be measured with stimuli of varying spatial frequencies. Mouse V1 neurons exhibit relatively low spatial resolution with a median preferred spatial frequency of ~0.035 cpd (cycles per degree), equivalent to a 2-D grating with a wavelength that extends ~28 degrees across visual space. This resolution is 10-15 times smaller than V1 cells of cats and primates, which respond best to a grating with a spatial frequency of ~ 1 and ~3 cpd, respectfully [89].

RETINOTOPIC ORGANIZATION

As one moves horizontally across the cortex from one cell to the next, their RF locations also shift smoothly across visual space [52,86]. Moreover, vertical columns of cells (those with somas aligned perpendicular to the cortical surface) tend to have overlapping receptive fields [63] **(Figure 7),** but it's important to note that there is considerable retinotopic scatter [86]. Nevertheless, the course scale retinotopic organization of V1 neurons is observed across mammals [3,89]. At a fine spatial scale, the RFs of neighboring V1 cells are scattered by ~5 degrees and thus are not perfectly retinotopically organized [82,86,87], although this scatter is smaller than the RFs of most mouse V1 cells.

CONTRAST POLARITY

The response of a simple cell in V1 can be elicited by two types of stimuli that fall within its spatial RF: a stimulus that increases its luminance (e.g., a bright spot) and one that decreases its luminance (e.g., dark spot). The ON subregion defines to portion of the RF that, when a bright spot appears, triggers a neural response. The OFF subregion is defined in a similar manner but with a dark stimulus. In simple cells, these two regions are usually spatially displaced (see below). The RFs of mouse V1 neurons often contain one to three localized subregions [65,73,74,81-86]

(**Figure 8**). Furthermore, the RFs of most L2/3 neurons contain two ON and OFF subregions, whereas those of L4 cells are dominated by only one type of polar contrast [83,85] **(Figure 8).**

Orientation

The majority of excitatory neurons in mouse V1 are tuned to the orientation of a stimulus, [45,52,54,68,73,81,83,86,90,91], particularly those residing in L4 and L2/3, where ~75% show sharp orientation tuning [81]. Unlike excitatory cells, most inhibitory V1 cells are broadly tuned to orientation [81,83,86]. As a population, the preferred orientation of mouse V1 neurons is generally uniform [45,81,90] , but an overrepresentation of the cardinal orientations has been observed [54,68], similar to populations of orientation tuned cells in the mouse dLGN.

Orientation Preference Maps

V1 of higher mammals (e.g., primates and carnivores) contains of vertical columns of cells with similar orientation preferences. The preferred orientation of cells within these columns smoothly changes, in a quasi-periodic fashion, as one moves horizontally across the cortical surface[92]. Vertical columns and horizontal maps of stimulus orientation are absent in V1 of rodents (but see reference [93]). Mouse V1 instead is said to contain a 'salt and pepper map' of orientation preferences, meaning that cells with similar or different orientation preferences can be found scattered within any region of the cortex [94].

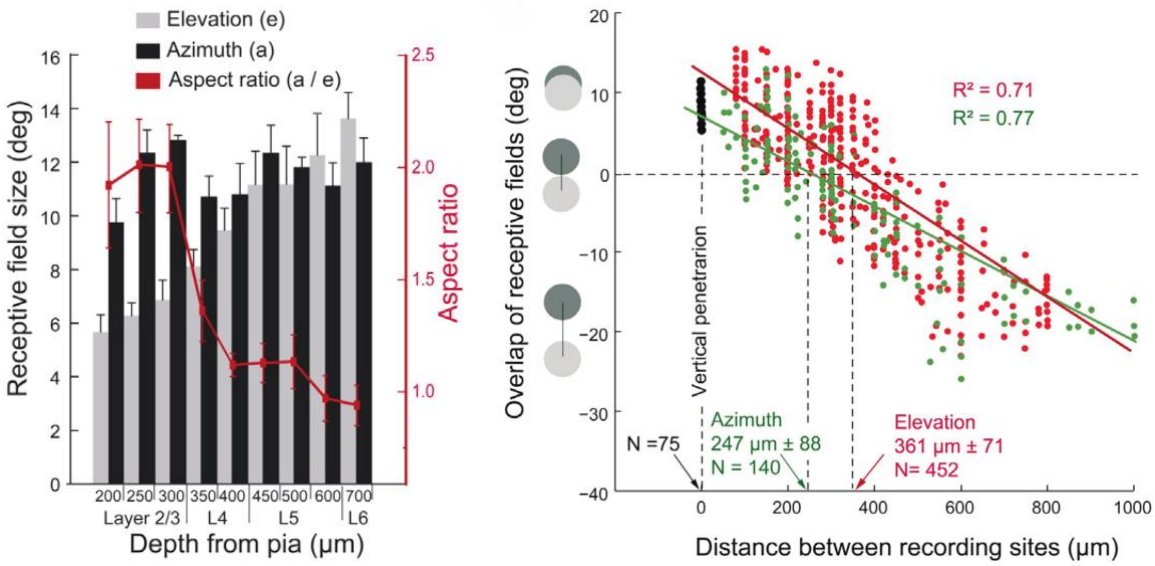

Figure 7 Spatial Tuning of V1 Neurons

***(LEFT)**: RFs are generally smaller (and their asymmetry is higher) in the upper layers of V1.*
***(RIGHT)** V1 cells residing within a cortical column (vertically aligned dots) have overlapping receptive fields, but also show some separation. V1 neurons are retinotopically organized along the azimuth (green lines) and elevation (red lines) dimension of visual space.*
Figure taken from Ji 2015.

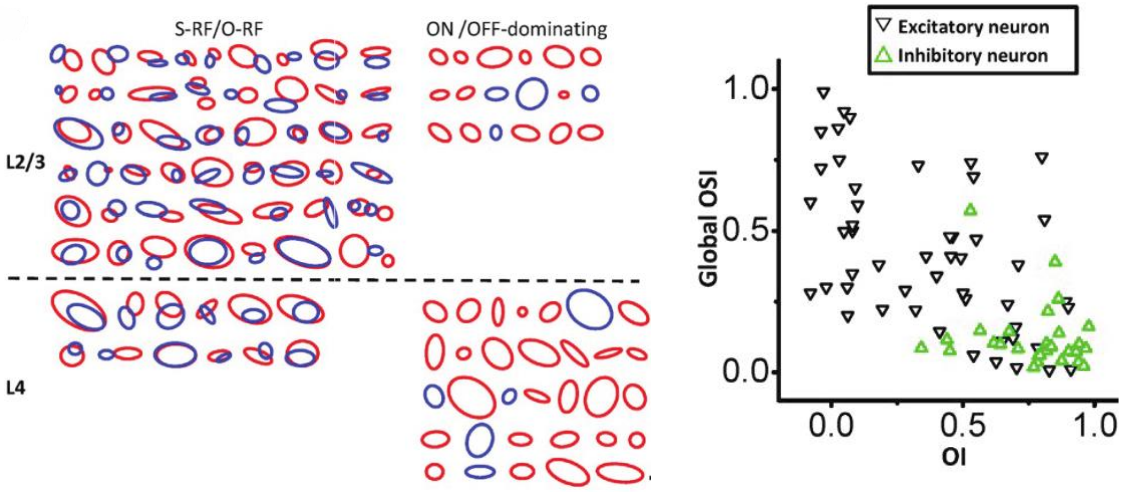

FIGURE 8 ORIENTATION TUNING AND SUBREGION OVERLAP

(LEFT) *L2/3 contains many excitatory cells with at least two subregions that vary in their overlap, while L4 is dominated by mono-contrast cells.*
(RIGHT) *Orientation selectivity (global OSI) becomes sharper as the ON and OFF subregions overlap (OL) decreases. Excitatory neurons (black triangles) can have separated or overlapping subregions, but those with segregated subfields generally have sharper orientation selectivity. Inhibitory neurons (green triangles) tend to be broadly tuned and have mostly overlapping subfields and untuned responses.*
Figure from Liu 2009.

SPACE VS. POLARITY VS. ORIENTATION TUNING

The subfields of cells in L2/3 can show some separation or be largely overlapping [82-84] while those of inhibitory neurons nearly always overlap [84,85] **(Figure 8).** In mouse V1, L2/3 cells with separate, side-by-side ON and OFF subfields [82,83] have sharper orientation tuning compared to those with overlapping subfields [83] (**Figure 8)**. Moreover, RFs of V1 cells in mice tend to have an elongated, elliptical structure [63-65,73,81-83] and these elliptical RFs can generally take on any orientation [64,65,81,86](**Figure 7, Figure 8)** reflecting the diversity of orientation preferences of V1 neurons [54,81]. Moreover, the RF structure of V1 cells can predict how they respond to the orientations of gratings [65,81]. Consistent with this notion, the neurons in deeper layers are have more symmetric RFs [63], and are less likely to be orientation tuned [81]. Similar to mice, orientation tuning of V1 neurons in other mammals can be predicted by the spatial arrangement of their ON-OFF subfields [50,95-99].

Simple vs Complex Cells

Some V1 neurons respond to the onset and offset of a stimulus in slightly separate locations of visual space, and the angle formed by the centers of the subfields can predict their orientation preference. These cells tend to show 'linear' response properties and traditionally are referred to as 'simple' cells. Those that respond both the onset and offset of a stimulus within the same visual field location tend to show non-linear responses and are referred to as complex cells [100] . However , this dichotomization is not absolute and is instead one of degree. In primates and carnivores simple cells dominate thalamic input L4, while those in upper layers are mostly complex [89] . In mice both L2/3 and L4 are dominated by simple cells, but a fair percentage of complex cells appear in both layers as well [81] .

THE THESIS

THE CHALLENGE

Simple cells in the primary visual cortex (V1) of all mammals are renown or having an 'orientation preference', meaning that they respond to a specific orientation of an elongated stimulus that reaches their receptive field (RF). Moreover, these simple cells respond to increments (e.g., light spots) and decrements (e.g., dark spots) in luminance in slightly separate regions of their RFs, and the angle formed by the centers of these regions can predict their preferred orientation.

Despite decades of research into the topic, the mechanism that gives rise to tuned simple cells and their highly structured RFs remains an open question. Many models struggle to explain why the properties of simple cells are similar across mammals, despite substantial inter-species differences in how these simple cells are spatially organized across the cortex. For instance, in V1 of cats and primate, vertical columns of cells have similar orientation preferences, and the preference of these columns rotates smoothly, in a quasiperiodic fashion, as one moves horizontally across the cortex. In contrast, simple cells in mouse V1 with different tuning preferences are scattered randomly throughout the cortical tissue.

Here I assess a mechanistic model of tuning, referred to as the *limited input model*, which may be able to explain how tuning emerges in different species. The model asserts that the retina is tiled by dipoles, which are ON- and OFF- center ganglion cells that signal the presence of 'lightness' and 'darkness' within a local region of visual space. The outputs of these dipoles are combined by simple cells in V1 endowing them with their orientation tuning. This mechanism is said to generate a diverse set of tuned cells that are either mapped out in an orderly manner across the cortex or arranged in a salt and pepper fashion.

In the following sections, I will describe the mechanism of the model and how it explains the tuning of simple cells in V1 of higher mammals, which contains a columnar map of orientation preferences, and how that same mechanism can explain tuning in V1 of mice, which exhibits a salt and pepper map of tuned cells. I will then describe a specific prediction made by the model: one should observe 'local tuning biases' among populations of cells in V1 of the mouse. Finally, I will provide an overview of the projects that were conducted to assess this prediction.

THE LIMITED INPUT MODEL

GENERATING TUNED SIMPLE CELLS

There are two key assertions made by the limited input model. First, in the retina, the nearest neighbor of an ON-center retinal ganglion cell (RGC) tends to be an OFF-center ganglion cell (and vice versa)[10,101,102] (**Figure 9, A and B**) . Thus one would frequently observe pairs of opposite sign RGCs that respond to 'dark spots' and 'light spots'. These pairs are referred to here as 'dipoles'. As illustrated in (**Figure 9B**), these dipoles form an angle and this angle varies across the retinal surface. Second, the model posits that simple cells in V1 are strongly driven by the signals of a single dipole. As a consequence, a given simple cell will acquire an orientation selective response and a preference that depends on the angle of the dipole that drives it (**Figure 9, Bottom**).

Thus, the limited input model claims that localized pairs of 'dark' and 'light' signals from the retina converge onto cortical simple cells endowing them with their tuning. Moreover, the model asserts that this mechanism can generate tuned cells that are either mapped out in an orderly manner across the cortex or arranged in a salt and pepper fashion, as described in the following sections.

GENERATING COLUMNAR MAPS OF ORIENTATION PREFERENCE

According to the model, orientation columns in higher mammals emerge because cells from the same column have highly overlapping RFs; consequentially, they are all dominated by inputs from the same retinal dipole and all will acquire a similar orientation preference determined by the angle of that dipole (**Figure 9, Top**).

Moreover, to explain the rotation of tuning preference of columns in higher mammals, the model posits that the angle of dipoles change smoothly as one moves across the retinal surface (**Figure 9, Top**). Given that neighboring dipoles send their signals to neighboring columns of V1 cells, the orientation preference of columns would smoothly change in a manner that matches the smoothly changing angle of the dipoles that tile the retinal surface [102,103] (**Figure 9**, **Top**).

GENERATING SALT AND PEPPER MAPS OF ORIENTATION PREFERENCE

The model can also explain orientation tuning of simple cells in mouse V1 which contains a salt and pepper map of tuning preferences. There are multiple ways that the model can be modified to achieve this. For example, by increasing the positional scatter of RGCs [102], or increasing the retinotopic scatter of mouse V1 populations [104] , the model will generate populations of sharply tuned cells organized in a salt and pepper manner.

In summary, the limited input model comes in two flavors. One version of the model generates orderly maps of tuning preferences that are observed in V1 of higher mammals, and another version produces the salt and pepper maps observed in mouse V1. Note that both versions give rise to simple cells that are tuned to orientation and whose RFs are composed of flanking ON- and OFF- subregions (**Figure 8, Left**).

PREDICTION: LOCAL TUNING BIASES

Most importantly, both versions of the model make the same assertion: The inputs to a simple cell in V1 are dominated by a single ON OFF dipole located within a specific region of the retina. This implies that all simple cells that pool from the same dipole will acquire an orientation preference that depends on the angle of the dipole they all pool from. That is, the model predicts that *neurons with overlapping RFs should have similar tuning*, a phenomena that will be referred to as 'local tuning biases'.

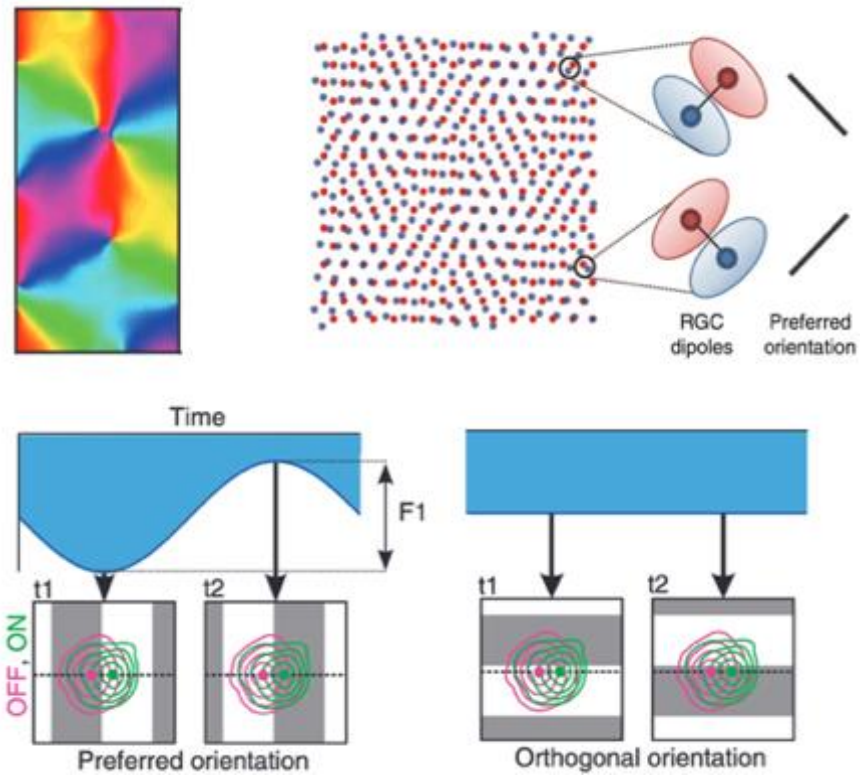

FIGURE 9 LIMITED INPUT MODEL OF ORIENTATION TUNING IN HIGHER MAMMALS

(TOP, LEFT) *A color map illustrating the cortical organization of orientation preferences across the surface of V1 in higher mammals. Each pixel corresponds to a vertical column of cells, and its color corresponds to the tuning preference of the cells in the column.* ***(TOP, RIGHT)*** *The grid of dots illustrates the receptive field locations of ON- (red) and OFF- (blue) center RGCs that tile the retinal surface. Local retinal regions contain pairs of ON- and OFF- center surround RGCs, with side by side RFs, referred to as 'dipoles'. The dipoles form an angle between them, and this angle varies across the retinal surface. In higher mammals, the angles of dipoles rotate smoothly as one moves across the retina. The response of a V1 neuron is dominated by the signals of a single dipole. This endows the neuron with an orientation preference that is perpendicular to the axis of the dipole that drives it.*

*(**BOTTOM**) An example of the response of a neuron that linearly combines the signals produced by a dipole to develop a preference to a stimulus orientation. When the dipole is stimulated by an oriented stimulus at a right angle to its axis (left), the cortical neuron responds robustly (F1), compared when the stimulus aligned with the axis of the dipole (right).*

(NOTE) *In higher mammals, cells within the same orientation column acquire the same tuning preference because they have overlapping RFs, that is, they are all dominated by signals of a single dipole. In higher mammals, moving across the surface of the cortex, the preference of columns smoothly change. The RFs of columns shift in a smooth manner across the cortical surface, so that they sample from a slightly different region of visual space. This leads to smooth shifts in the angle of the dipole a cortical column pools from, and therefore a smooth change in their orientation preference.*

Figure (A) taken from Paik and Ringach 2011; figure (B) adapted from Lien and Scanziani 2013;

AIMS

The limited input model is fairly successful in explaining how tuning emerges in V1 of mammals that have orderly maps of orientation preferences [102]. However, there is a lack of physiological data from the mouse that corroborates the version of model that generates salt and pepper maps seen in mouse V1. The goal of this thesis is to fill in this gap.

PRIMARY AIMS

To test whether the model can explain how tuning emerges in mice, I test a specific prediction made by the limited input model: *one should observe local tuning biases in populations of mouse V1 cells. That is, cells with overlapping RFs should have similar tuning*. This prediction is assessed in **Project 1 – Local Tuning Biases in Mouse Primary Visual Cortex (Chapter 3)**.

Second, this thesis aims to determine the origin of the local tuning biases observed in mouse V1. One idea is that they are inherited from the dLGN (the subcortical structure that provides the bulk of the input to V1). To test this, I search for local tuning biases in the tuned LGN afferents that innervate mouse V1. This assessment is conducted in **Project 2 – Local Tuning Biases in the Mouse Lateral Geniculate Nucleus (Chapter 4)**.

SUPPLEMENTARY AIMS

The thesis also addresses some supplementary questions. First is to determine how 'darkness' and 'lightness' are represented by local populations of V1 neurons in the mouse, and how it compares to that of V1 neurons of higher mammals. In primates, cats and humans, decreases in the luminance of a stimulus generate stronger cortical responses than increments in luminance; that is, responses to dark spots are stronger than responses light spots [105]. Moreover, in cat, populations of V1 cells have OFF subregions that tend to be clustered together, while their ON subregions show more retinotopic scatter. Whether mouse V1 populations exhibit these ON- vs OFF- asymmetries is addressed in **Project 1 – Local Tuning Biases in Mouse Primary Visual Cortex (Chapter 3)**.

How the cortex devotes resources to analyze stimuli at each point in visual space is an outstanding question in visual neuroscience. A traditional, long-standing view posits that each region of space is processed by a set of filters tuned to a diverse range of preferences, and that this process is repeated for each point in space [92,106,107]. The limited input model assessed in this thesis rejects this view, and instead posits that cortical populations responding to different regions of the image do not process these regions in the same manner [102,103,108]. The functional implications of this claim are discussed in **Project 1 – Local Tuning Biases in Mouse Primary Visual Cortex (Chapter 3)**.

Finally, I discuss some potential mechanisms that can give rise to the unidirectional and axis selectivity in the mouse dLGN in **Project 2 – Local Tuning Biases in the Mouse Lateral Geniculate Nucleus (Chapter 4)**.

LOCAL TUNING BIASES IN MOUSE PRIMARY VISUAL CORTEX

LUIS O. JIMENEZ [1], **ELAINE TRING** [2], **JOSHUA T. TRACHTENBERG** [2], **AND DARIO L. RINGACH** [1,2]

[1]Department of Psychology, University of California, Los Angeles, California;
[2]Department of Neurobiology, David Geffen School of Medicine, University of California, Los Angeles, California

J NEUROPHYSIOLOGY 120: 274–280, 2018.
First published April 18, 2018; doi:10.1152/jn.00150.2018
RAPID REPORT Sensory Processing

ABSTRACT

Neurons in primary visual cortex are selective to the orientation and spatial frequency of sinusoidal gratings. In the classic model of cortical organization, a population of neurons responding to the same region of the visual field but tuned to all possible feature combinations provides a detailed representation of the local image. Such a functional module is assumed to be replicated across primary visual cortex to provide a uniform representation of the image across the entire visual field. In contrast, it has been hypothesized that the tiling properties of ON- and OFF-center receptive fields in the retina, largely mirrored in the geniculate, may constrain cortical tuning at each location in the visual field. This model predicts the existence of local biases in tuning that vary across the visual field and would prevent the cortex from developing a uniform, modular representation as postulated by the classic model. Here, we confirm the existence of local tuning biases in the primary visual cortex of the mouse, lending support to the notion that cortical tuning may be constrained by signals from the periphery.

SIGNIFICANCE

Populations of cortical neurons responding to the same part of the visual field are shown to have similar tuning. Such local biases are consistent with the hypothesis that cortical tuning, in mouse primary visual cortex, is constrained by signals from the periphery.

INTRODUCTION

Mice lack the precise spatial organization of neural preferences into radial columns and two-dimensional feature maps that are a hallmark of cat and monkey primary visual cortex (area V1; Grinvald et al. 1986; Hübener et al. 1997; Ts'o et al. 1990). Instead, neurons with diverse tuning preferences intermingle in the cortex to form "salt-and-pepper" maps (Bonin et al. 2011; Ohki et al. 2005; Van Hooser 2007). Despite this apparent disorder, the receptive field properties and tuning of individual neurons in mouse V1 are similar to those of their counterparts in higher mammals (Bonin et al. 2011; Lien and Scanziani 2013; Niell and Stryker 2008; Vaiceliunaite et al. 2013). In particular, they show similar tuning for the orientation and spatial frequency of sinusoidal gratings (Ringach et al. 2016). How populations of neurons in mouse V1 represent a local image and how such representation compares with that of higher mammals are central questions of visual neuroscience (Mazade and Alonso 2017; Van Hooser 2007).

The classic model of V1 in higher mammals posits that populations of neurons with overlapping receptive fields, comprising a hypercolumn, develop a full set of tuning preferences, such as all possible orientations and spatial frequencies (Hubel and Wiesel 1977). A cortical hypercolumn would then have all the machinery required to represent local image structure accurately (Daugman 1988). An alternative model of cortical organization postulates that the spatial tiling of ON/OFF receptive fields in the retina, and largely mirrored in the geniculate (Usrey et al. 1999), constrains cortical tuning at each location in the visual field (Ringach 2004, 2011, 2013; Soodak 1987). This model predicts the existence of local tuning biases that ought to be reflected in a tendency for the similarity of tuning between neurons to increase with a measure of their receptive field overlap. Here, we report evidence of a correlation between receptive field overlap and tuning similarity in primary visual cortex of the mouse, lending support to the notion that cortical tuning may be, in part, determined by biases originating in the periphery (Ringach 2013).

RESULTS

We measured the visual properties of neurons in primary visual cortex using resonant, two-photon microscopy in the awake, behaving mouse (Fig. 1*A*). To measure the tuning of neurons to orientation and spatial frequency, we used a visual stimulus consisting of a sequence of flashed, high-contrast sinusoidal gratings having pseudorandom orientations and spatial frequencies **(Figure 10, *top***). We estimated the tuning of each cell by linearly regressing the response on the stimulus **(Figure 10C).** We denote the estimated tuning kernel of the $i-th$ cell in the population by h_t^i. As expected, cells were selective for orientation and band pass in spatial frequency (Niell and Stryker 2008). We define the tuning similarity between a pair of cells as the correlation coefficient between their tuning kernels $d_T^{ij} = \langle h_t^i, h_t^j \rangle / \|h_t^i\| \|h_t^j\|$ **(Figure 10C)**. The peak of the tuning curve also yielded a preferred orientation and spatial frequency (**Figure 10C).**

We also measured the location of receptive fields in visual space using a sparse noise stimulus in which dark and bright disks were randomly flashed on the computer screen for a brief period before being relocated (Figure 10B, *bottom*). We computed separate ON and OFF maps for each cell by correlating their responses with the location of the bright and dark disks, respectively (Jones and Palmer 1987; Figure 10D). We denote the ON/OFF maps corresponding to the $i-th$ cell in the population by h_{on}^{i} and h_{off}^{i}, respectively. We define the index of overlap between ON/OFF subregions, $d_{on}^{ij}$and d_{off}^{ij}, as the correlation coefficients of their respective maps (Figure 10D). The distribution of preferred orientations shows a slight overrepresentation of the cardinal directions (Figure 10E), and the distribution of the preferred spatial frequencies had a log-normal shape, with a geometric mean of 0.04 cycles/° (Figure 10F). The results are consistent with previous reports (Kondo and Ohki 2016; Niell and Stryker 2008).

Interestingly, the average overlap of OFF subregions in a small cortical neighborhood (cells within 100 µm of each other) is significantly higher than ON subregions (Figure 10G; n_{on} = 1,340, n_{off} = 2,729, medians of 0.24 and 0.42 for ON and OFF, respectively, Wilcoxon rank sum test, $P = 1.1 \times 10^{-59}$). Moreover, there is a slight dominance of OFF over ON responses ((Figure 10H; Wilcoxon sign rank test, $n = 679$, $P = 3.9 \times 10^{-9}$; see METHODS). The relatively lower scatter of OFF compared with ON subregions and the slight dominance of OFF responses in the superficial layers of the cortex are two organizational features that resemble what is observed in higher mammals (Jin et al. 2008; Kremkow et al. 2016; Lee et al. 2016; Yeh et al. 2009).

Our central finding is that there is a highly significant, positive correlation between tuning similarity and receptive field overlap (ON subregions, $n = 209$, $r = 0.38$, $P = 2.4 \times 10^{-8}$; OFF subregions, $n = 790$, $r = 0.32$, $P = 2.9 \times 10^{-21}$; ON/OFF subregions, $n = 999$, $r = 0.38$, $P = 2.7 \times 10^{-36}$;Figure 11). We defined groups of cell pairs with low and high overlap as those falling within the first and fourth quartiles of the overlap index distribution, respectively (Figure 11A). Tuning similarity for cells with receptive fields with low overlap was significantly lower than that with receptive fields with high overlap (Figure 11A, *top* histograms; median values of −0.03 and 0.39, Wilcoxon ranked-sum test, $P = 6.2 \times 10^{-30}$). The correlation between tuning similarity and receptive field overlap was significant in four out of the six mice when tested individually ($P < 0.01$). The two mice that failed to show an effect had the lowest number of cell pairs ($n = 15$ and 61). Four cell pairs showing different degrees of overlap and tuning similarity are shown in Figure 11B.

To probe the robustness of our finding, we also explored different measures of receptive field overlap and tuning similarity. A different measure of receptive field overlap is the normalized distance, defined as the distance between the peaks of receptive fields divided by the average, effective radius of their sizes. The size of a receptive field was defined as the area >90% of its maximum value. The normalized distance can be computed separately for both ON and OFF maps. We find that the median normalized distance of ON subregions is significantly greater than those of OFF subregions (Figure 12A; n_{on} = 1,340, n_{off} = 2,729, medians of 2.34 and 1.69 for ON and OFF subregions, respectively; rank sum test, $P = 5.6 \times 10^{-32}$), consistent with our earlier result (Figure 12G). Finally, tuning similarity correlates with normalized distance [Figure 12B; $r = -0.24$, $P = 1.6 \times 10^{-15}$, solid curve is an exponential fit $y = Ae^{-bx}$, with $A = 0.40$ (0.33, 0.47) and $b = 0.37$ (0.26, 0.48), optimal fit values and 95% confidence intervals in parentheses]. Next, for each cell, we defined the composite sum map as $h_{on+off} = h_{on} + h_{off}$ and a composite difference map as $h_{on+off} = h_{on} - h_{off}$. We defined the overlap measure d_{on+off} as the correlation

coefficient between the composite sum maps of two cells and the measure $d_{\text{on−off}}$ as the correlation coefficient between the composite difference maps. We find that tuning similarity is correlated with both $d_{\text{on+off}}$ (Figure 12C; $r = 0.38$, $P = 2.5 \times 10^{-41}$) and $d$on−off (Figure 12D; $r = 0.22$, $P = 2.5 \times 10^{-14}$). The weaker correlation with overlap based on difference maps arises from the fact that the composite difference maps tend to have increased amount of noise in background, which biases the values of correlation coefficients toward 0. We also find that the similarity of preferred orientation (Figure 12E; $r = -0.16$, $P = 2.9 \times 10^{-8}$) and spatial frequencies (Figure 12F; $r = -0.15$, $P = 2.5 \times 10^{-7}$) is significantly correlated with $d_{\text{on+off}}$. However, it is clear the strength of the correlation is not as high as seen when we measure tuning similarity based on the shapes of the full tuning kernels.

Altogether, the data demonstrate the existence of local tuning biases, where cells with high degree of receptive field overlap tend to have higher tuning similarity than cells with low degrees of overlap.

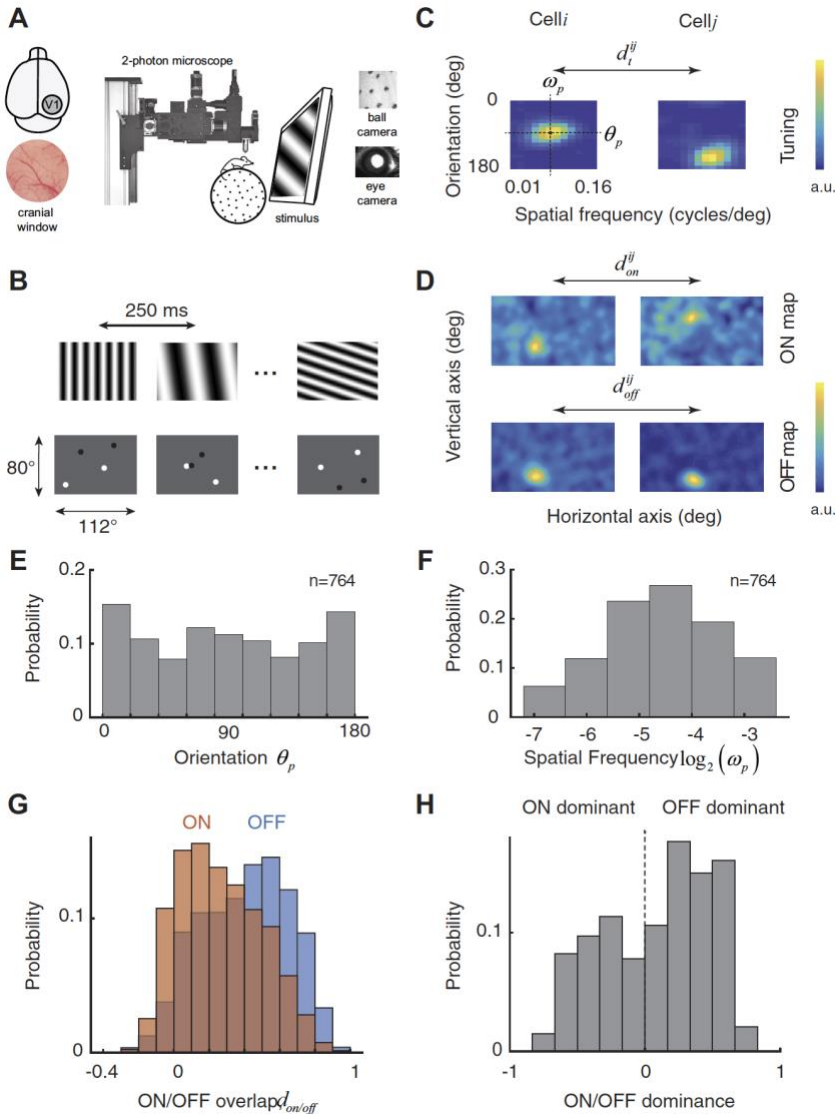

FIGURE 10 EXPERIMENTAL SETUP AND BASIC MEASURES OF RECEPTIVE FIELDS AND TUNING SELECTIVITY

(A): *experimental setup: 2-photon imaging in awake behaving mouse. A cranial window is implanted over the primary visual cortex (area V1). Mice are head-restrained but otherwise free to walk, rest, or groom on a spherical treadmill. Eye movements and locomotion are monitored by cameras synchronized to the microscope.* ***(B)*** *pseudorandom sequences of full-field, sinusoidal gratings were used to map the tuning for orientation and spatial frequency. Sparse noise stimuli consisting of randomly flashed dark and bright disks were used to map the ON and OFF subregions of each cell.* ***(C)*** *2 examples of tuning kernels in the orientation and spatial frequency domain. Kernels are normalized and presented in arbitrary units (a.u.). Spatial frequency was sampled in equal steps in a logarithmic scale. From the kernels, we estimate the preferred orientation of the cell, θ_p, as well as its preferred spatial frequency, ω_p. Similarity between the tuning kernels of 2 cells, i and j, is denoted by d_t^{ij}. deg, Degrees.* ***(D)*** *2 examples of ON and OFF maps. Kernels are normalized and presented in arbitrary units. Dimensions of the image in visual space correspond to the ones displayed in B. Similarities between ON and OFF maps of 2 cells, i and j, are denoted by d_{on}^{ij} and d_{off}^{ij}, respectively.* ***(E)*** *distribution of preferred orientation in the population. There is a slight overrepresentation of the cardinal orientations.* ***(F)*** *distribution of preferred spatial frequency.* ***(G)*** *distribution of ON and OFF subregion overlap in cells 100 m apart from each other. There is a higher scatter for ON than OFF subregions.* ***(H)*** *histogram of the relative amplitudes of ON and OFF kernels shows a slight dominance of OFF responses.*

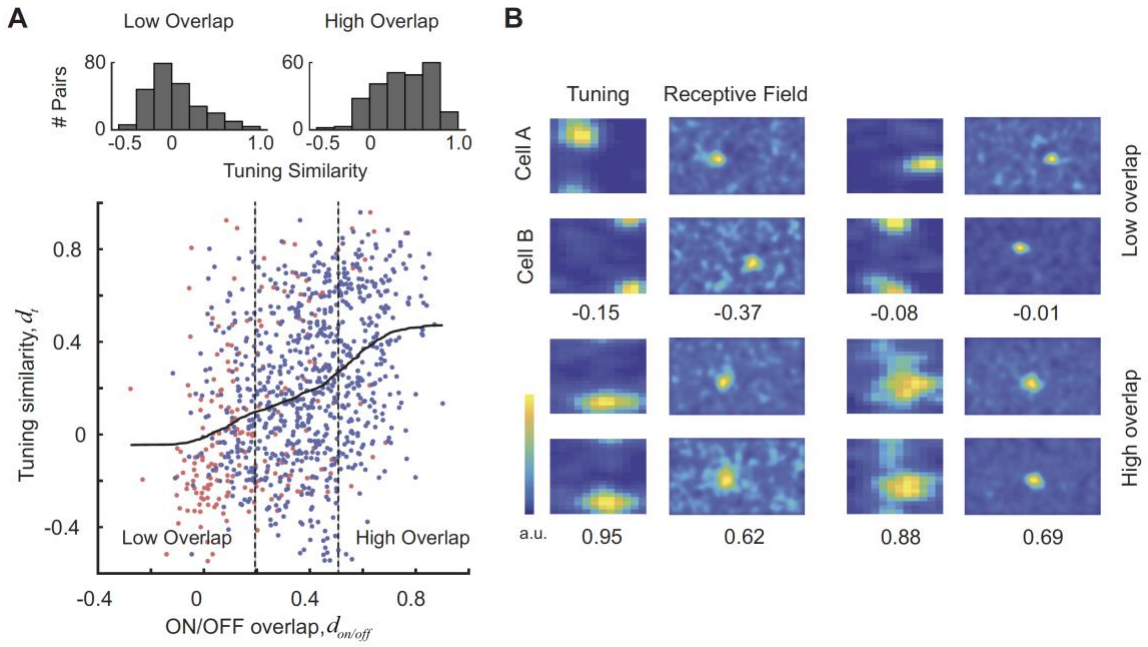

FIGURE 11 EVIDENCE OF LOCAL TUNING BIAS IN MOUSE PRIMARY VISUAL CORTEX.

(A, bottom): *tuning similarity (d_t) is positively correlated with receptive field overlap of both ON and OFF subregions (d_{on} and d_{off}). Scatterplot shows tuning similarity against the overlap of ON or OFF subregions. Pairs of cells may be plotted twice, once showing the overlap of ON subregions (red points) and once showing the overlap with OFF subregions (blue points). Solid curve represents a smoothed version of the scatterplot obtained via local regression.*

(A Top): *histograms of tuning similarity values for pairs with low and high overlap (defined by the vertical, dashed lines). Pairs with high degree of receptive field overlap have a significantly higher similarity of tuning than pairs with low degree of receptive field overlap. #, Number of.*

(B)*examples of 4 cell pairs with different degrees of receptive field overlap and tuning similarity. For each pair, the tuning similarity and receptive field overlap values are shown at the bottom. Top row shows examples of cell pairs with low degree of receptive field overlap and tuning similarity. Bottom row shows examples of cell pairs with high degree of receptive field overlap and tuning similarity.*

a.u., Arbitrary units.

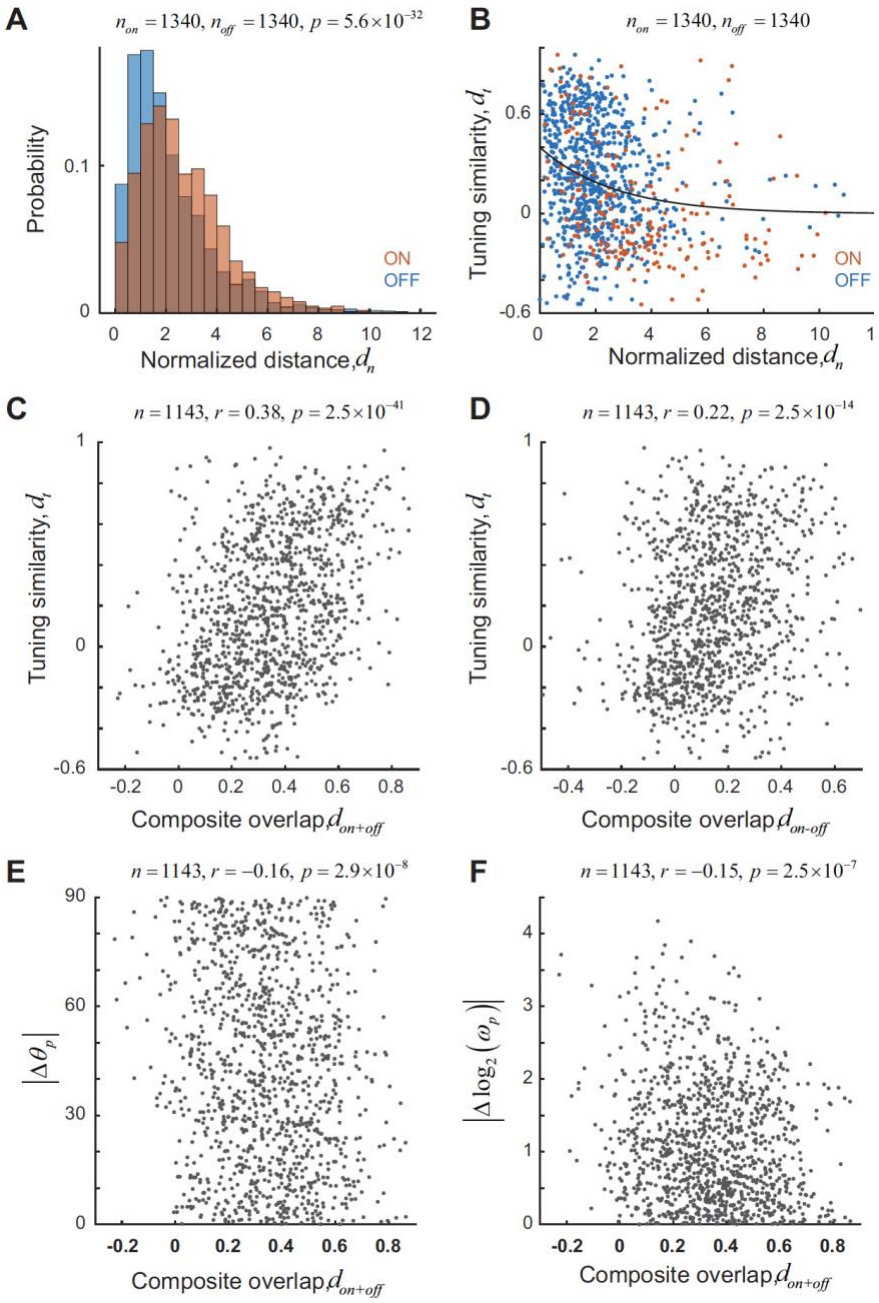

FIGURE 12 ROBUSTNESS OF CORRELATION BETWEEN TUNING SIMILARITY AND RECEPTIVE FIELD OVERLAP.

(A) *distribution of normalized distance (d_n), a measure of receptive field overlap, for ON (red) and OFF (blue) subregions for pairs <100 μm apart on the cortex. ON subregions show larger positional scatter.*

(B) *tuning similarity is inversely correlated with normalized distance. Solid line represents an exponential fit to the data. Receptive fields with overlapping receptive fields tend to have higher tuning similarity than receptive fields that are far apart in the visual field. Blue dots represent OFF subregions. Red dots represent ON subregions.*

(C and D): *tuning similarity is correlated with receptive field overlap measures based on the sum (d_{on+off})or difference (d_{on+off}) of ON and OFF maps.*

(E and F)*: absolute differences of preferred orientation ($|\Delta\,\theta_p\,|$) and spatial frequency ($|\Delta log_2(\,\omega_p)\,|$) are correlated with receptive field overlap based on the sum of ON and OFF maps.*

DISCUSSION

Local tuning biases imply that populations of neurons responding to different parts of the visual field do not represent the local image in a uniform way, as assumed by modular cortical organization. The preferences of a population of neurons responding to one location of the visual field will be biased to one specific combination of orientation and spatial frequency, whereas populations responding to other locations will have a different bias. How can the cortex reconstruct the structure of the image given such incomplete information?

To draw an analogy, the situation is like the structure of the photoreceptor mosaic, where at any one retinal position we may find an L, M, or S cone. In other words, the retinal representation does not offer all three spectral measurements at each position. Nevertheless, a partial set of measurements along with the statistical regularities of natural scenes allow the brain to infer the image most likely to have produced a particular pattern of activation across the cone mosaic (Brainard 2015). A cortical representation where different parts of the visual field are represented by populations of cells with different tuning biases offers a similar challenge, and a similar solution based on the statistics of natural scenes can be offered.

In the mouse, at least three different factors may exert a tuning bias onto the cortex. First, there is a specialized circuit carrying direction-selective signals that arise in retinal ganglion cells. These cells target the lateral geniculate nucleus (LGN) "shell," which, in turn, projects to the superficial layers of the cortex (Cruz-Martín et al. 2014). If some cells preferentially sample from one of these inputs, they are expected to inherit the same selectivity and location in the visual field. A different type of projection from the retina to cortex occurs via the core of the LGN and innervates layers 4 and 6. Recent studies reveal that geniculate afferents from the core are moderately tuned for the orientation and direction of a stimulus (Kondo and Ohki 2016; Piscopo et al. 2013; Sun et al. 2016). Thus it may be possible that some cortical cells reflect the biases of these individual thalamic inputs. At the same time, differences in the tuning of layer 4 neurons and their thalamic inputs indicate that not all cortical selectivity is inherited by sampling of individual LGN afferents. Cells in layer 4 have a band-pass spatial frequency tuning with peak spatial frequencies higher than those of thalamic afferents (Kondo and Ohki 2016). Layer 4 neurons also show higher selectivity than those of thalamic afferents and have a larger diversity of preferred orientations, whereas LGN inputs are biased heavily toward the cardinals (Kondo and Ohki 2016). Thus one can expect the structure of a population of simple cell receptive fields in layer 4 to arise from the combination of spatially displaced ON- and OFF-center thalamic afferents, as described in the classic Hubel and Wiesel (1977) model. When ON- and OFF-center receptive fields are combined in this way, tuning biases can still arise when their available number of inputs is limited or spatially unbalanced. Note that the relationship between tuning similarity and receptive field overlap holds separately for ON and OFF subregions (Figure 11). In principle, a pair of simple cells could share just one subregion but still have very different orientation tuning. The fact that this is not observed is consistent with a scenario where a limited set of inputs constrains cortical tuning (Ringach 2011).

The next natural step would be to determine whether a comparable relationship exists in higher mammals. In cats, we know the sum of geniculate ON/OFF receptive fields converging onto a cortical column is biased, and the "population receptive field" profile resembles that of a simple

cell with a preferred orientation that matches the preference of the target cortical column (Jin et al. 2011). Although this finding is partly consistent with local tuning biases, it leaves open the possibility that a nearby cortical column has a different tuning preference while responding to the same location in the visual field. A second study reported that cells with orientation preferences 90° apart could only be found if the centers of the corresponding receptive fields were at least one receptive field diameter apart in the visual field (Das and Gilbert 1997). Those findings have been controversial (Bosking et al. 2002) but are consistent with our results and deserve further consideration. If local tuning biases can be demonstrated in higher mammals, the data would favor a broader role of peripheral guidance in the development of cortical tuning and maps across species (Ringach 2004, 2011, 2013; Soodak 1987).

METHODS

Animals. All procedures were approved by the University of California, Los Angeles, Office of Animal Research Oversight (the Institutional Animal Care and Use Committee) and were in accord with guidelines set by the US National Institutes of Health. A total of 6 C57BL/6J mice (The Jackson Laboratory), both male (3) and female (3), aged postnatal days 35–56, were used in this study. Mice were housed in groups of 2 or 3, in reversed light cycle. Animals were naïve subjects with no prior history of participation in research studies. We imaged 26 different fields to obtain the data discussed in this paper.

Surgery. Carprofen and buprenorphine analgesia were administered preoperatively. Mice were then anesthetized with isoflurane (4–5% induction; 1.5–2% surgery). Core body temperature was maintained at 37.5°C using a feedback heating system. Eyes were coated with a thin layer of ophthalmic ointment to prevent desiccation. Anesthetized mice were mounted in a stereotaxic apparatus. Blunt ear bars were placed in the external auditory meatus to immobilize the head. A portion of the scalp overlying the two hemispheres of the cortex (~8 × 6 mm) was then removed to expose the underlying skull.

After the skull was exposed, it was dried and covered by a thin layer of Vetbond. After the Vetbond dried (~15 min), it provided a stable and solid surface to affix the aluminum bracket with dental acrylic. The bracket was then affixed to the skull, and the margins were sealed with Vetbond and dental acrylic to prevent infections.

Virus injection. A 3-mm-diameter region of skull overlying the occipital cortex was removed. Care was taken to leave the dura intact. GCaMP6-fast (University of Pennsylvania Vector Core: AAV1.Syn.GCaMP6f.WPRE.SV40; #AV-1-PV2822) was expressed in cortical neurons using adeno-associated virus (AAV). AAV-GCaMP6- fast (titer: ~10^{13} genomes/ml) was loaded into a glass micropipette and slowly inserted into the primary visual cortex (V1) using a micromanipulator. Two injection sites were made centered around the center of V1 and separated ~200 µm apart. For each site, AAV-GCaMP6-fast was pressure-injected using a Picospritzer III (4 puffs at 15–20 psi with a duration of 10 ms, and each puff was separated by 4 s; Parker, Hollis, NH) starting at a depth of 350 µm below the pial surface and making injections every 10 µm moving up with the last injection made at 100 µm below the pial surface. The total volume injected across all depths was ~0.5 µl. The injections were made by a computer program in control of the micromanipulator and the Picospritzer.

A sterile 3-mm-diameter cover glass was then placed directly on the dura and sealed at its edges with Vetbond. When dry, the edges of the cover glass were further sealed with dental acrylic. At the end of the surgery, all exposed skull and wound margins were sealed with Vetbond and dental acrylic, and a small, sealed glass window was left in place over the occipital cortex. Mice were then removed from the stereotaxic apparatus, given a subcutaneous bolus of warm sterile saline, and allowed to recover on the heating pad. When fully alert, they were placed back in their home cage.

Imaging. Once expression of GCaMP6f was observed in primary visual cortex, typically between 11 and 15 days after the injection, imaging sessions took place. Imaging was performed using a resonant, two-photon microscope (Neurolabware, Los Angeles, CA) controlled by Scanbox acquisition software (Los Angeles, CA). The light source was a Coherent Chameleon Ultra II

laser (Santa Clara, CA) running at 920 nm. The objective was a ×16 water immersion lens (0.8 numerical aperture, 3-mm working distance; Nikon). The microscope frame rate was 15.6 Hz (512 lines with a resonant mirror at 8 kHz). Eye movements and pupil size were recorded via a Dalsa Genie M1280 camera (Teledyne Dalsa) fitted with a 740-nm long-pass filter that looked at the eye indirectly through the reflection of an infrared-reflecting glass. Images were captured at an average depth of 260 μm.

Visual stimulation. Sequences of pseudorandom sinusoidal gratings (Malone and Ringach 2008; Ringach et al. 1997) and sparse noise stimuli were generated in real- time by a Processing sketch using OpenGL shaders (see https://processing.org). In generating pseudorandom gratings, the orientation domain was sampled in equal steps of 10° for a total of 18 possible orientations; the spatial frequency domain was sampled in equal steps on a logarithmic scale from 0.0079 to 0.1549 cycles/°, for a total of 12 possible spatial frequencies; and for each combination of orientation and spatial frequency, spatial phase was equally sampled in steps of 45°, leading to a total of 8 possible settings. The tuning curves were computed by averaging responses over spatial phase, as done in previous studies (Malone and Ringach 2008; Ringach et al. 2002). The duration of the sequences was either 20 or 30 min, and gratings were updated 4 times a second on a screen refreshed at 60 Hz. Thus each combination of orientation and spatial frequency appeared ≥22 times on average (for a 20-min sequence). Sparse noise consisted of flashed dark and bright disks with a diameter of 5°. Two disks of each contrast appeared at any one time. The lifetime of each disk was 250 ms, after which it was removed and repositioned randomly on the screen. Transistor-transistor logic signals generated by the stimulus computer were sampled by the microscope and time-stamped with the frame and line number being scanned at that time. The time stamps provided the synchronization between visual stimulation and imaging data.

In all experiments, we used a BenQ XL2720Z screen, which measured 60 × 34 cm and was viewed at 20-cm distance, subtending 112 × 80° of visual angle. The screen was calibrated using a Photo Research (Chatsworth, CA) PR-650 spectroradiometer, and the result was used to generate the appropriate γ-corrections for the red, green, and blue components via an NVIDIA Quadro K4000 graphics card. The contrast of the stimulus was 80%. The center of the monitor was positioned with the center of the receptive field population for the eye contralateral to the cortical hemisphere under consideration. The locations of the receptive fields were estimated by an automated process where localized, flickering checkerboard patches appeared at randomized locations within the screen. This experiment was run at the beginning of each imaging session to ensure the centering of receptive fields on the monitor. We imaged the monocular region of V1 in the left hemisphere. The receptive fields of neurons were centered around 20–35° in azimuth and 0–20° in elevation on the right visual hemifield.

Image processing. The image processing pipeline was the same as described in detail elsewhere (Ringach et al. 2016). Briefly, calcium images were aligned to correct for motion artifacts. Following motion stabilization, we used a MATLAB (MathWorks, Natick, MA) graphical user interface tool developed in our laboratory to define regions of interest corresponding to putative cell bodies manually. Following segmentation, we extracted signals by computing the mean of the calcium fluorescence within each region of interest and discounting the signals from the nearby neuropil. Spikes were then estimated via deconvolution (Berens et al. 2018).

Kernel estimation. The estimation of the tuning kernel was performed as in earlier studies by fitting a linear model between the response and the stimulus (Ringach et al. 2016). Similarly, we computed the ON/OFF maps by fitting a linear model between the response and the location of

bright and dark spots. The maps were smoothed with the Gaussian window of $\sigma = 5°$. For each cell, we used the map at the optimal time delay between stimulus and response. The optimal delay was defined as the time at which the variance of the kernel reached its maximum. A tuning kernel was defined as significant if the peak variance was at least two times that of the baseline measured at negative time lags. ON and OFF maps showed a distribution of values that was close to normal. We defined the optimal delay time as the one at which the map kurtosis reached its maximum. We considered a map significant if its peak kurtosis was >8. The results described below were robust to the selection of these thresholds.

Tuning similarity and overlap indices. The similarity of tuning between two cells was defined as the cross-correlation coefficient between their tuning kernels. In some cases, we also investigated the similarity orientation preference, defined by the absolute difference between the preferred orientations, or the similarity of their peak spatial frequency, defined as the absolute difference of the logarithm (base 2) of the preferred frequency. The preferred parameters were computed as the center of mass of horizontal (for spatial frequency) and vertical (for orientation) slices of the tuning kernel passing through the peak response (Fig. 1C). As a measure of overlap between ON and OFF subregions, we computed the correlation coefficient between the maps. In some analyses, we also computed a normalized overlap measure between receptive field pairs, defined as the distance between the locations of their peaks normalized by the mean square root of their areas. The area of a receptive field was defined by the size of the region >90% of the maximum response. When assessing a statistical correlation between indices of overlap and tuning similarity, we used Spearman rank correlation, as these are bounded indices that are not normally distributed. The smoothed version of the scatterplot in Figure 11E was generated by local regression using weighted least squares and a 1st degree polynomial model (as implemented by smooth function in MATLAB).

An ON/OFF dominance index was defined based on the peak amplitudes of the corresponding kernels, A_{off} and A_{on}, by the equation $(A_{off} - A_{on})/(A_{off} + A_{on})$. An index of +1 corresponds to a cell with a pure, dominant OFF subregion, an index of −1 corresponds to a cell with a pure, dominant ON subregion, and an index of 0 represents a cell with perfectly balanced ON and OFF responses. A Wilcoxon rank sign test was used to test the null hypothesis that the distribution is balanced.

GRANTS

D. L. Ringach was supported by National Eye Institute Grant EY-018322 and National Institute of Biomedical Imaging and Bioengineering Grant EB-022915, and J. T. Trachtenberg was supported by National Eye Institute Grant EY-023871.

REFERENCES

Berens P, Freeman J, Deneux T, Chenkov N, McColgan T, Speiser A, Macke JH, Turaga SC, Mineault P, Rupprecht P, Gerhard S, Friedrich RW, Friedrich J, Paninski L, Pachitariu M, Harris KD, Bolte B, Machado TA, Ringach D, Stone J, Rogerson LE, Sofroniew NJ, Reimer J, Froudarakis E, Euler T, Román Rosón M, Theis L, Tolias AS, Bethge M. Community-based benchmarking improves spike rate inference from two-photon calcium imaging data. *PLoS Comput Biol* 14: e1006157, 2018. doi:10.1371/journal.pcbi.1006157. [PMCID: PMC5997358] [PubMed: 29782491] [CrossRef: 10.1371/journal.pcbi.1006157]

Bonin V, Histed MH, Yurgenson S, Reid RC. Local diversity and fine-scale organization of receptive fields in mouse visual cortex. *J Neurosci* 31: 18506–18521, 2011. doi:10.1523/JNEUROSCI.2974-11.2011. [PMCID: PMC3758577] [PubMed: 22171051] [CrossRef: 10.1523/JNEUROSCI.2974-11.2011]

Bosking WH, Crowley JC, Fitzpatrick D. Spatial coding of position and orientation in primary visual cortex. *Nat Neurosci* 5: 874–882, 2002. doi:10.1038/nn908. [PubMed: 12195429] [CrossRef: 10.1038/nn908]

Brainard DH. Color and the cone mosaic. *Annu Rev Vis Sci* 1: 519–546, 2015. doi:10.1146/annurev-vision-082114-035341. [PubMed: 28532367] [CrossRef: 10.1146/annurev-vision-082114-035341]

Cruz-Martín A, El-Danaf RN, Osakada F, Sriram B, Dhande OS, Nguyen PL, Callaway EM, Ghosh A, Huberman AD. A dedicated circuit links direction-selective retinal ganglion cells to the primary visual cortex. *Nature* 507: 358–361, 2014. doi:10.1038/nature12989. [PMCID: PMC4143386] [PubMed: 24572358] [CrossRef: 10.1038/nature12989]

Das A, Gilbert CD. Distortions of visuotopic map match orientation singularities in primary visual cortex. *Nature* 387: 594–598, 1997. doi:10.1038/42461. [PubMed: 9177346] [CrossRef: 10.1038/42461]

Daugman JG. Complete discrete 2-D Gabor transforms by neural networks for image analysis and compression. *IEEE Trans Acoust* 36: 1169–1179, 1988. doi:10.1109/29.1644. [CrossRef: 10.1109/29.1644]

Grinvald A, Lieke E, Frostig RD, Gilbert CD, Wiesel TN. Functional architecture of cortex revealed by optical imaging of intrinsic signals. *Nature* 324: 361–364, 1986. doi:10.1038/324361a0. [PubMed: 3785405] [CrossRef: 10.1038/324361a0]

Hubel DH, Wiesel TN. Ferrier lecture. Functional architecture of macaque monkey visual cortex. *Proc R Soc Lond B Biol Sci* 198: 1–59, 1977. doi:10.1098/rspb.1977.0085. [PubMed: 20635] [CrossRef: 10.1098/rspb.1977.0085]

Hübener M, Shoham D, Grinvald A, Bonhoeffer T. Spatial relationships among three columnar systems in cat area 17. *J Neurosci* 17: 9270–9284, 1997. doi:10.1523/JNEUROSCI.17-23-09270.1997. [PMCID: PMC6573591] [PubMed: 9364073] [CrossRef: 10.1523/JNEUROSCI.17-23-09270.1997]

Jin J, Wang Y, Swadlow HA, Alonso JM. Population receptive fields of ON and OFF thalamic inputs to an orientation column in visual cortex. *Nat Neurosci* 14: 232– 238, 2011. doi:10.1038/nn.2729. [PubMed: 21217765] [CrossRef: 10.1038/nn.2729]

Jin JZ, Weng C, Yeh CI, Gordon JA, Ruthazer ES, Stryker MP, Swadlow HA, Alonso JM. On and off domains of geniculate afferents in cat primary visual cortex. *Nat Neurosci* 11: 88–94, 2008. doi:10.1038/nn2029. [PMCID: PMC2556869] [PubMed: 18084287] [CrossRef: 10.1038/nn2029]

Jones JP, Palmer LA. An evaluation of the two-dimensional Gabor filter model of simple receptive fields in cat striate cortex. *J Neurophysiol* 58: 1233–1258, 1987. doi:10.1152/jn.1987.58.6.1233. [PubMed: 3437332] [CrossRef: 10.1152/jn.1987.58.6.1233]

Kondo S, Ohki K. Laminar differences in the orientation selectivity of geniculate afferents in mouse primary visual cortex. *Nat Neurosci* 19: 316–319, 2016. doi:10.1038/nn.4215. [PubMed: 26691830] [CrossRef: 10.1038/nn.4215]

Kremkow J, Jin J, Wang Y, Alonso JM. Principles underlying sensory map topography in primary visual cortex. *Nature* 533: 52–57, 2016. doi:10.1038/nature17936. [PMCID: PMC4860131] [PubMed: 27120164] [CrossRef: 10.1038/nature17936]

Lee KS, Huang X, Fitzpatrick D. Topology of ON and OFF inputs in visual cortex enables an invariant columnar architecture. *Nature* 533: 90–94, 2016. doi:10.1038/nature17941. [PMCID: PMC5350615] [PubMed: 27120162] [CrossRef: 10.1038/nature17941]

Lien AD, Scanziani M. Tuned thalamic excitation is amplified by visual cortical circuits. *Nat Neurosci* 16: 1315–1323, 2013. doi:10.1038/nn.3488. [PMCID: PMC3774518] [PubMed: 23933748] [CrossRef: 10.1038/nn.3488]

Malone BJ, Ringach DL. Dynamics of tuning in the Fourier domain. *J Neurophysiol* 100: 239–248, 2008. doi:10.1152/jn.90273.2008. [PMCID: PMC2493484] [PubMed: 18480369] [CrossRef: 10.1152/jn.90273.2008]

Mazade R, Alonso JM. Thalamocortical processing in vision. *Vis Neurosci* 34: E007, 2017. doi:10.1017/S0952523817000049. [PMCID: PMC5716341] [PubMed: 28965507] [CrossRef: 10.1017/S0952523817000049]

Niell CM, Stryker MP. Highly selective receptive fields in mouse visual cortex. *J Neurosci* 28: 7520–7536, 2008. doi:10.1523/JNEUROSCI.0623-08.2008. [PMCID: PMC3040721] [PubMed: 18650330] [CrossRef: 10.1523/JNEUROSCI.0623-08.2008]

Ohki K, Chung S, Ch'ng YH, Kara P, Reid RC. Functional imaging with cellular resolution reveals precise micro-architecture in visual cortex. *Nature* 433: 597–603, 2005. doi:10.1038/nature03274. [PubMed: 15660108] [CrossRef: 10.1038/nature03274]

Piscopo DM, El-Danaf RN, Huberman AD, Niell CM. Diverse visual features encoded in mouse lateral geniculate nucleus. *J Neurosci* 33: 4642–4656, 2013. doi:10.1523/JNEUROSCI.5187-12.2013. [PMCID: PMC3665609] [PubMed: 23486939] [CrossRef: 10.1523/JNEUROSCI.5187-12.2013]

Ringach DL. Haphazard wiring of simple receptive fields and orientation columns in visual cortex. *J Neurophysiol* 92: 468–476, 2004. doi:10.1152/jn.01202.2003. [PubMed: 14999045] [CrossRef: 10.1152/jn.01202.2003]

Ringach DL. Peripheral guidance of cortical organization. In: *The New Visual Neurosciences*, edited by Werner JS and Chalupa LM. Cambridge, MA: MIT Press, 2013. Ringach DL. You get what you get and you don't get upset. *Nat Neurosci* 14: 123–124, 2011. doi:10.1038/nn0211-123. [PubMed: 21270775] [CrossRef: 10.1038/nn0211-123]

Ringach DL, Bredfeldt CE, Shapley RM, Hawken MJ. Suppression of neural responses to nonoptimal stimuli correlates with tuning selectivity in macaque V1. *J Neurophysiol* 87: 1018–1027, 2002. doi:10.1152/jn.00614.2001. [PubMed: 11826065] [CrossRef: 10.1152/jn.00614.2001]

Ringach DL, Mineault PJ, Tring E, Olivas ND, Garcia-Junco-Clemente P, Trachtenberg JT. Spatial clustering of tuning in mouse primary visual cortex. *Nat Commun* 7: 12270, 2016. doi:10.1038/ncomms12270. [PMCID: PMC4974656] [PubMed: 27481398] [CrossRef: 10.1038/ncomms12270]

Ringach DL, Sapiro G, Shapley R. A subspace reverse-correlation technique for the study of visual neurons. *Vision Res* 37: 2455–2464, 1997. doi:10.1016/S0042- 6989(96)00247-7. [PubMed: 9381680] [CrossRef: 10.1016/S0042-6989(96)00247-7]

Soodak RE. The retinal ganglion cell mosaic defines orientation columns in striate cortex. *Proc Natl Acad Sci USA* 84: 3936–3940, 1987. doi:10.1073/pnas.84.11.3936. [PMCID: PMC304991] [PubMed: 3108884] [CrossRef: 10.1073/pnas.84.11.3936]

Sun W, Tan Z, Mensh BD, Ji N. Thalamus provides layer 4 of primary visual cortex with orientation- and direction-tuned inputs. *Nat Neurosci* 19: 308–315, 2016. doi:10.1038/nn.4196. [PMCID: PMC4731241] [PubMed: 26691829] [CrossRef: 10.1038/nn.4196]

Ts'o DY, Frostig RD, Lieke EE, Grinvald A. Functional organization of primate visual cortex revealed by high resolution optical imaging. *Science* 249: 417–420, 1990. doi:10.1126/science.2165630. [PubMed: 2165630] [CrossRef: 10.1126/science.2165630]

Usrey WM, Reppas JB, Reid RC. Specificity and strength of retinogeniculate connections. *J Neurophysiol* 82: 3527–3540, 1999. doi:10.1152/jn.1999.82.6.3527. [PubMed: 10601479] [CrossRef: 10.1152/jn.1999.82.6.3527]

Vaiceliunaite A, Erisken S, Franzen F, Katzner S, Busse L. Spatial integration in mouse primary visual cortex. *J Neurophysiol* 110: 964–972, 2013. doi:10.1152/jn.00138.2013. [PMCID: PMC3742980] [PubMed: 23719206] [CrossRef: 10.1152/jn.00138.2013]

Van Hooser SD. Similarity and diversity in visual cortex: is there a unifying theory of cortical computation? *Neuroscientist* 13: 639–656, 2007. doi:10.1177/1073858407306597. [PubMed: 17911223] [CrossRef: 10.1177/1073858407306597]

Yeh CI, Xing D, Shapley RM. "Black" responses dominate macaque primary visual cortex V1. *J Neurosci* 29: 11753–11760, 2009. doi:10.1523/JNEUROSCI.1991- 09.2009. [PMCID: PMC2796834] [PubMed: 19776262] [CrossRef: 10.1523/JNEUROSCI.1991-09.2009]

LOCAL TUNING BIASES IN MOUSE LATERAL GENICULATE NUCLEUS

INTRODUCTION

Introduction

Simple cells in the primary visual cortex (V1) are selective to multiple properties of images, most notably the location and orientation of edge-like features within a local region [92] . Neurons with these orientation tuned responses are present in V1 of all known mammals [89] suggesting that they are fundamental for visual processing [89].

Despite the importance and decades of research into the topic, the mechanism that generates tuning remains an open question. Part of the debate regards how orientation tuning is generated in *individual* simple cells, and how this mechanism relates to the process that generates the organization of tuned cortical *populations* [51]. For example, in higher mammals, vertical columns of cells show similar orientation preferences, and the preference of these columns rotates smoothly, in a quasiperiodic fashion, as one moves horizontally across the cortex [50,92]. However, in V1 of the mouse, neurons have larger receptive fields, and cells with different tuning preferences are scattered randomly across the cortical tissue [94]. Despite these variations across species the general structure of the spatial receptive fields (RFs) and the orientation selectivity of simple cells remains constant [81].

Another open question is whether the process that generates tuning in mouse V1 is similar to the process that generates the tuning of neurons in the mouse dorsal lateral geniculate nucleus (dLGN). The mouse retina is populated by a subclass of retinal ganglion cells (RGCs) that respond robustly to stimulus movement along one of the cardinal directions [6] . The mouse dLGN also contains these cardinal-direction tuned cells and, in addition, is populated by cells that are selective to both directions that form an axis (e.g., both upward *and* downward motion) [34,53] . In all, these observations pose a challenge to models which must explain how or if orientation tuning in V1 is implemented in a similar fashion across different species and across different visual regions [56].

Tuning vs Retinotopy

A family of models, inspired by the work of Hubel and Wiesel [92] suggest that the feedforward convergence of ON and OFF signals onto cortical population of cells endows them with their orientation tuning. These models make predictions regarding the relationship between orientation tuning of neurons and their spatial receptive fields [2,102,108]. One particular model posits that cells

representing the same local image regions have similar tuning preference [102,103,109]. A myriad of recent studies of local populations of cells in mouse V1 corroborate this notion. In mouse V1, cells with overlapping RFs have highly correlated activity over long periods of stimulation [72,86] and, in turn, cells with such strong correlations tend to have similar orientation preferences [86]. Furthermore, V1 neurons with similar RFs are likely to be strongly bidirectionally connected, and these strongly wired cells tend to share orientation preferences [72-74]. Excitatory connected V1 neurons, known share similar orientation preferences [74], are also driven by the same thalamic afferent [62], perhaps because they are driven by signals from a similar region of visual space.

More evidence that local retinal regions are represented by a biased set of tuned cells comes from studies of 'sibling' neurons (i.e., clonally related cells derived from the same progenitor cell). Sibling neurons are connected via electrical junctions early in development causing them to form strong chemical synapses and similar tuning preferences in adulthood [68,78-80]. In an effort to simulate the development of these sibling cells, Ko and colleagues [73] designed a neural network of cells that, prior to training, were connected via these electrical junctions. During training, sibling cells acquired highly similar RFs leading to two consequences: The activity of siblings became highly correlated, and they developed strong bilateral connections, both of which are traits of cells that are tuned to the same orientation [68,72-74,78-80]. Thus, the developmental model suggests that sibling neurons with similar RFs are destined to acquire similar tuning preferences. Furthermore, a recent pair of studies revealed that mouse superior colliculus (SC) contains vertical columns of cells with similar orientation preferences, but each of these columns only cover a specific portion of the visual field which do not overlap with the RFs of other columns [55,110]. In conclusion, studies of multilaminar V1 networks, among others [62,71], support the notion that cells representing the same point of visual space are constrained to have the same tuning preference.

THE CURRENT STUDY

Recently, we found more evidence of local tuning biases in mouse V1, such that cells that have overlapping ON or OFF subregions have similar orientation and spatial frequency tuning [109]. The source of these local tuning biases remains an open question. One idea is that they are inherited from the thalamus, and possibly, that the thalamus inherits its local tuning biases from the retina (**Figure 15**). Here we assess whether such local tuning biases exist the mouse dLGN, known to contain direction, axis, and spatial frequency tuned neurons [34,45-48,53] which project tuned afferents [39,54] to V1. Using in vivo-two photon imaging, we estimated the linear spatial RF maps and joint orientation and spatial frequency tuning of thalamic afferents innervating mouse V1. We find a significant relationship between the RF overlap and tuning similarity of these geniculate inputs. Our findings corroborate the notion that local tuning biases of thalamic afferents originate from the retina and are relayed onto the V1, preventing cortical populations from representing local regions of visual space with a diverse set of tuning profiles [111].

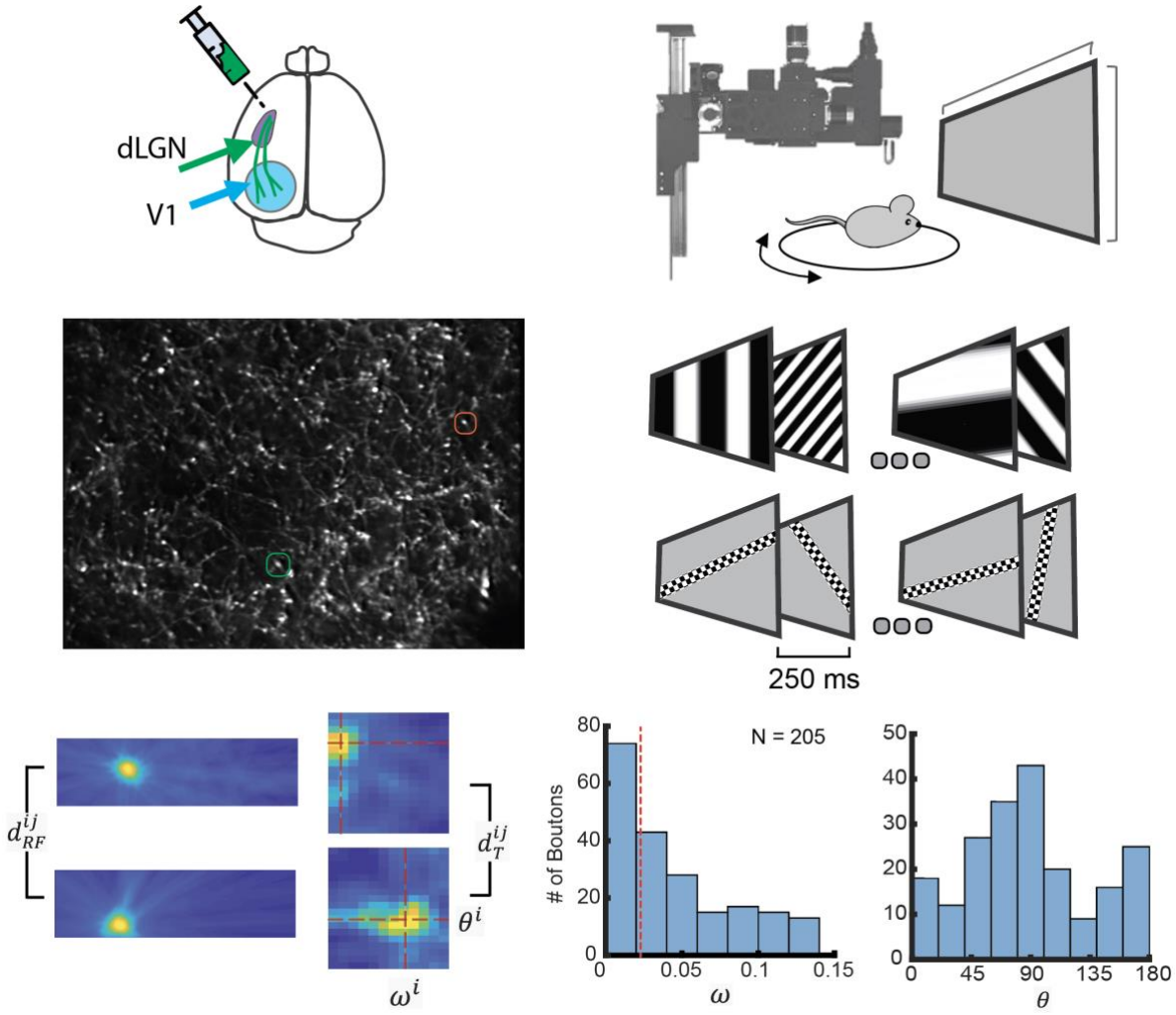

FIGURE 13 TUNING, RF MAPS, AND THEIR SIMILARITIES, OF DLGN BOUTONS.

(A, top) *Injection of GcaMP6s in the dLGN using an AAV leads to expression in thalamic afferents innervating V1.*
(A, bottom) *Example snapshot of a population of GcaMP6s expressing boutons innervating mouse V1.*
(B) *In vivo two-photon calcium imaging of dLGN afferents in V1 during visual stimulation. Mice are head-restrained but otherwise free to walk, rest, or groom on a spherical treadmill while viewing stimuli shown in (C).*
(C, Top) *Pseudorandom sequences of full-field sinusoidal gratings were used to map the tuning of boutons for orientation and spatial frequency.* ***(C, Bottom)*** *To estimate RF maps of boutons, a sequence of elongated bars were flashed at different locations and orientations across the screen.*
(D) *Example of RF maps, joint tuning kernels and their similarities for two dLGN boutons, i and j, from the same imaging field shown in (A, bottom). Maps and kernels are normalized and presented in arbitrary units. The overlap between RF maps and similarity of tuning kernels, between two boutons i and j is denoted by* d_{RF}^{ij} *and* d_T^{ij}*, respectively. For each bouton, the preferred orientation of the cell,* θ_i*, and its preferred spatial frequency,* ω_i*, is taken from the peak of the tuning kernel.*
*(****E, left****) Histogram of spatial frequency preferences of dLGN boutons with significant tuning kernels. Red vertical line denotes the median value of 0.028 cycles per degree.* ***(E, right)*** *Histogram of preferred orientations preferences of dLGN boutons with significant tuning kernels. There is a strong bias towards cardinal orientations*

RESULTS

We expressed GcaMP6s in dLGN boutons innervating L2/3 and L4 of mouse primary visual cortex and measured their visual properties using resonant, two-photon microscopy in the awake, behaving mouse (**Figure 13**).

A bouton's joint tuning to orientation and spatial frequency was measured by presenting a sequence of flashed, high-contrast sinusoidal gratings having pseudorandom orientations and spatial frequencies (**Figure 13**). We estimated the tuning of each bouton by linearly regressing its response on the grating stimulus and denote the estimated tuning kernel of the ith bouton in an imaging field by H_T^i. The peak of the tuning kernel also yielded a spatial frequency preference ω_i and an orientation preference θ_i for each bouton (see methods, **Figure 13**).

We also measured the spatial receptive field maps of boutons by presenting a sequence of flickering, elongated bars at random orientations and positions across the visual field (**Figure 13**). A boutons RF map was estimated by correlating its response and the location of the bars. We denote the RF map corresponding to the ith bouton in an imaging field by H_R^i.

We find that dLGN boutons innervating mouse primary visual cortex are orientation and spatial frequency selective and the distribution of preferred orientations has a bias for cardinal orientations. (**Figure 13).**

To assess the existence of local tuning biases of dLGN inputs to mouse V1, we asked if boutons with overlapping RFs have similar joint tuning profiles. We define the tuning similarity of bouton pairs as the as the correlation between their joint tuning kernels $d_T^{ij} = \langle H_T^i, H_T^j \rangle / \|H_T^i\| \|H_T^j\|$. The RF overlap of bouton pairs is defined as the correlation coefficient between their RF maps $d_R^{ij} = \langle H_R^i, H_R^j \rangle / \|H_R^i\| \|H_R^j\|$. We find a significant positive correlation between the joint tuning similarity of bouton pairs and the overlap between their RFs (r = 0.29, p=9.5 x 10^{-5}, n = 178) (**Figure 14**).

As a further test, we assessed the distribution of joint tuning similarity of boutons with high RF overlap and compared to those with low RF overlap. Bouton pairs with RF correlations that fell within the first and fourth quartile of the RF correlation distribution were deemed to have RFs with high and low overlap, respectively (**Figure 14**). The joint tuning similarity of boutons with high RF overlap was significantly greater than those with low RF overlap (median d_T^{ij} with high RF overlap = 0.79, median d_T^{ij} with low RF overlap = 0.28, Wilcoxon ranked-sum 2-tailed test, P= 7 x 10^{-6} ; (**Figure 14**). Both scatter plots shown in (**Figure 14**) and have regression lines that are bounded by a 95% confidence interval. The left vertical line and right vertical lines of the scatter plots denote the 25th and 75th percentile of the RF correlation distribution, respectively.

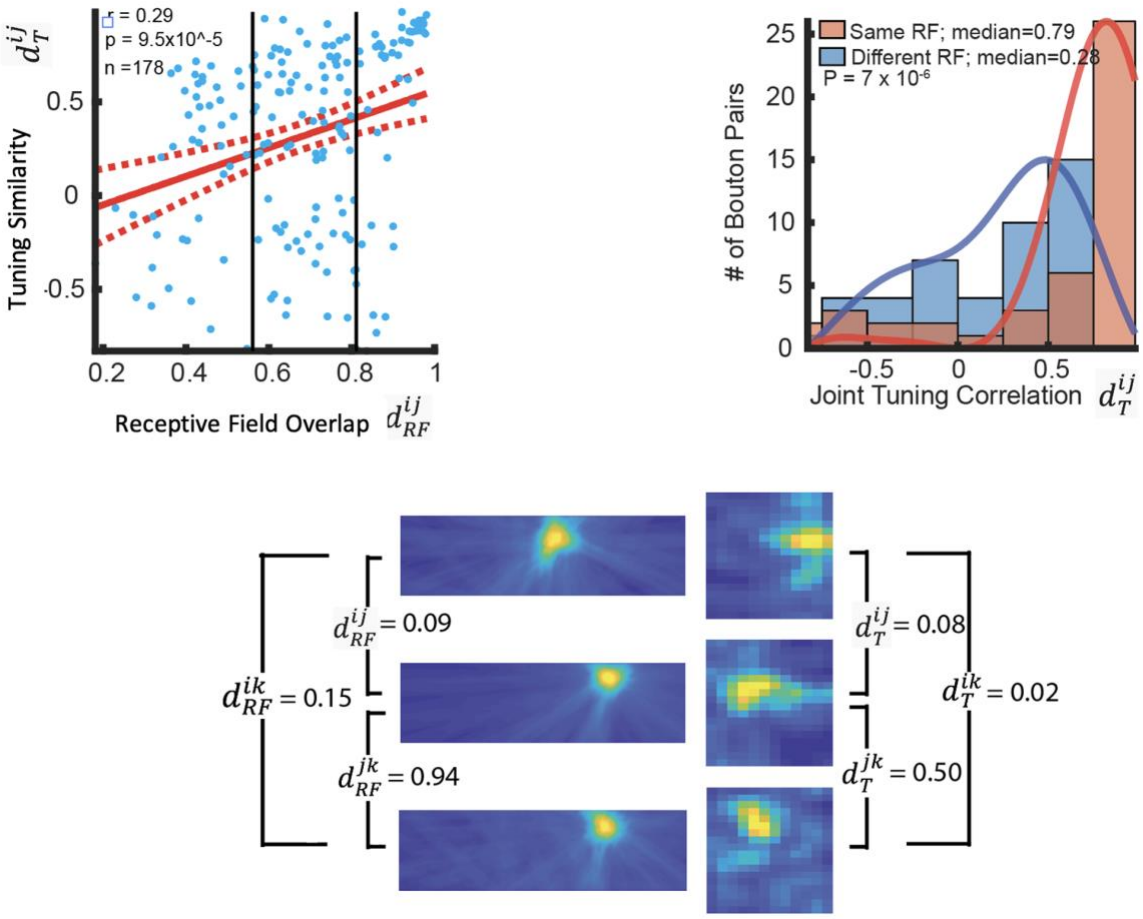

FIGURE 14 EVIDENCE OF LOCAL TUNING BIASES IN DLGN BOUTONS INNERVATING MOUSE V1

(Top left) *Scatter plot and fitted regression line showing a positive correlation between tuning similarity and RF overlap, for all boutons in the data set (5 fields, 3 mice total).*

(Top right) *Histogram of joint tuning similarity for bouton pairs with overlapping (blue) and non-overlapping (red) RFs. Bouton pairs with overlapping RF (red) have a significantly higher tuning similarity (Median = 0.34) than those with different RFs (Median = 0.21)*

(Bottom) *RFs maps (left column) and tuning kernels (right column) for three boutons I (top row), j (middle row) and k (bottom row) from the same imaging session. Middle and bottom boutons, j and k, have overlapping receptive fields and similar tuning. The top bouton, i, has a different RF and different tuning kernel than those of boutons j and k.*

DISCUSSION

We find that individual thalamic afferents are slightly less selective compared to the outputs of cortical cells **(Figure 13),** as reported in another study [54] (although see reference [39]). Our main finding is that thalamocortical afferents with overlapping RFs do not have a diverse set of tuning profiles and are instead biased towards a specific orientation and spatial frequency. These biases resemble the local tuning biases observed in V1 we reported in an earlier study [109], where cells with overlapping RFs have similar tuning profiles. These results suggests that local tuning biases in mouse V1 can be inherited from biases in their thalamic inputs.

There are at least three mechanisms that can explain the local tuning biases observed in the primary visual cortex and thalamic afferents. Thalamic neurons may acquire their similar and overlapping RFs if they all combine the inputs from the same spatially neighboring pair of ON and OFF center RGCs (**Figure 15A**), or if they all are driven by the same direction tuned RGC (**Figure 15 B**). In both of these scenarios, thalamic cells or cortical cells with overlapping RFs would have similar tuning. A third scenario is that untuned center surround thalamic cells with spatially offset ON- and OFF- subregions converge onto multiple cortical targets, endowing them with the same tuning preference and similar receptive fields (**Figure 15C**)

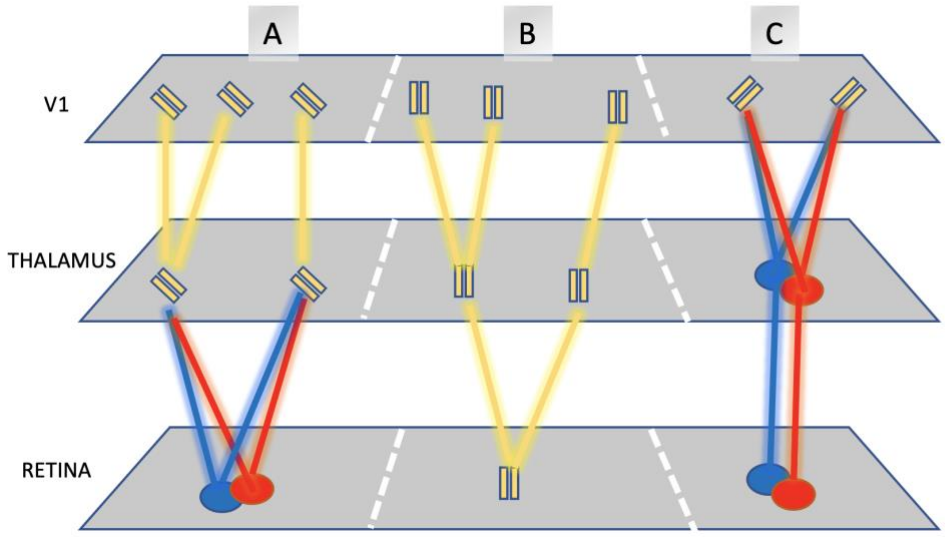

FIGURE 15 THREE POSSIBLE MECHANISMS THAT GENERATE LOCAL TUNING BIASES IN THALAMIC AFFERENTS OR THEIR CORTICAL TARGETS

(A) *Thalamic cells acquire similar tuning (i.e., show local tuning biases) by receiving convergent input from a pair of neighboring ON- and OFF- center RGCs. In turn, these thalamic cells project their tuned afferents and innervate multiple cortical cells.*
(B) *A direction tuned RGC endows its thalamic targets with a similar direction preference direction, and these thalamic neurons relay the same tuned signal onto multiple cortical targets.*
(C) *A the axons of a pair untuned thalamic cells with spatially offset ON- and OFF subfields converge onto multiple cortical cells.*
In mechanism A and B, but not C, thalamic afferents could also exhibit local tuning biases. In all three cases, cortical simple cells will exhibit local tuning biases.

ORIENTATION TUNING OF SINGLE CELLS IN THE DLGN

Assuming the different thalamic afferents we measured belonged to different thalamic cells, our results show that thalamic neurons with similar RFs are likely to have similar tuning. This suggests that the dLGN also represents local image regions with a biased set of orientation tuned cells, similar to recent findings of the mouse SC [55,110]. Why would groups of dLGN cells pooling inputs from the same retinal region have similar tuning preferences?

Traditionally, the thalamus is said to lack cells that are tuned to stimulus orientation [21,50,51]. In mice however, this is clearly not the case. Some neurons in the dLGN, especially those in the shell region **(Figure 5**), are clearly tuned [9,33,34,39,48,52], either to movement along a single direction (e.g., the upward movement only), or along an axis (e.g., both upward *and* downward movement) [9,33,34,39,45,46,48,53,54].

INHERITANCE OF TUNING FROM THE RETINA

Causal evidence supports the notion that cells in the mouse SC directly inherit their tuning from RGCs selective to motion along the one of the cardinal directions [15]. These findings have inspired the idea that direction tuned dLGN cells also acquire their tuning from direction selective RGC inputs [21,39,45,90] (**Figure 15 B**). Similarly, axis selectivity in the dLGN is proposed to emerge from the thalamic pooling of RGC inputs that are tuned to opposite motion directions [21,33,53,112].

However, models of dLGN tuning that invoke the pooling of direction tuned RGCs face some challenges. For instance, orientation tuning in mouse V1 remains relatively intact in transgenic mouse lines with deficits in retinal directional selectivity [113], suggesting that tuning in the dLGN does not depend on direction tuned inputs from the retina.

Moreover, it is not clear how thalamic cells that are tuned to a *single direction* avoid combining a large number of diverse inputs tuned to multiple directions. Promiscuous pooling of a large number of diverse inputs would likely preclude orientation selectivity of dLGN neurons. This is problem evident in inhibitory V1 neurons which are poorly selective due to pooling the inputs of neurons with a diversity of tuning preferences [60].

Similarly, it is not known how dLGN cells tuned to a specific *axis* of motion can specifically 'pick and choose' RGCs with opposite motion preferences. Even if axis selective dLGN neurons are able to specifically pool only from RGC inputs with opposing motion preferences (see reference [53]), it is not clear how their tuning would remain sharp given that these motion signals conflict and can 'cancel' each other out. For instance, human psychophysical experiments show that motion percepts are lost when observers view stimuli moving in opposite direction within in local visual regions [114].

POOLING OF ON/OFF RGCS

Another possibility is that that tuning in the dLGN is generated de-novo, for example, dLGN neurons can their tuning by pooling from spatially displaced ON- and OFF center surround RGCs [65,101] (**Figure 15 A**).

Direction Tuning

Direction tuning in the dLGN can emerge via a Reichardt type mechanism, in which a dLGN neuron pools from center-surround RGCs with side-by-side RFs and different temporal

dynamics. This is a plausible mechanism given that center surround RGCs, with transient and sustained responses [6,19], form the majority of axons that that project to the dLGN [34] . Moreover, these Reichardt computations are implemented by the bipolar-to-amacrine retinal network across the animal kingdom [4,115,116] and can possibly explain how layer 4 neurons in mouse V1 acquire their direction tuning [49].

Axis Tuning

Axis tuning in the dLGN can also be accomplished if a dLGN neuron pools from a pair of spatially offset, center-surround RGCs with the same temporal response pattern. A dLGN neuron that combines such inputs would show robust responses to stimuli moving in both opposing motion directions that form an axis [65]. This idea consistent with findings showing that the responses of some dLGN neurons to the orientation of gratings can be predicted by the orientation of their RFs, although with considerable error [46,48,56] .

LIMITED INPUT

Regardless of how direction or axis tuning emerges, a unresolved question is exactly how thalamic cells 'pick and choose' an appropriate set of retinal inputs. If dLGN cells inherit their direction or axis tuning from direction tuned RGCs, how do they avoid combining a too many RGCs tuned to a diverse set of directions? Or if dLGN neurons acquire their tuning by combining the inputs of neighboring ON- and OFF center surround cells , how do they avoid selecting inputs with largely separate RFs? One explanation is that thalamic neurons are compelled to select an appropriate set of RGCs, simply because the number of RGC inputs available to them is limited. Restricting the size of the retinal input pool would effectively constrain the diversity tuning profiles a thalamic cell can build [101,117] (**Figure 16**). If dLGN cells are given only a few inputs to choose from, they will be less likely to pool a diverse range of different motion signals, or pool center surround inputs with inappropriately arranged RFs. Indeed, a random wiring model that assumes that inputs are limited [53] appears to explain the emergence of direction and axis tuning in the dLGN [53]. Moreover, a limited input scenario is expected to endow postsynaptic cells with overlapping RFs with similar tuning, consistent with the local tuning biases we observed here and those observed in the SC [55,110].

CONCLUSION

Note that we did not estimate the ON- or OFF- subregions of thalamic afferents. Therefore, we are not able to determine if local tuning biases in mouse V1 could emerge due to the convergence of center surround, untuned inputs (**Figure 15 C**).. However, there is developing evidence that thalamic afferents with spatially offset subregions or different temporal response patterns converge onto a common cortical cell to endow it with axis [65] or direction [49] tuning.

Another drawback is our inability to ensure that thalamic boutons originated from different thalamic cells. Although this was an issue, note that the RF maps of afferents, as well as their tuning kernels, showed great diversity (**Figure 14**). Also consider that in mice, there is a relatively large number of distinct thalamic axons that target the same cortical region (5000 afferents/mm2)[32]. It is therefore likely that we imaged thalamocortical afferents belonging to a large number of thalamic cells.

Finally, note that the correlation between RF overlap and tuning similarity is slightly weaker in the dLGN afferents than that we observed in V1 [109] (r = 0.29 in dLGN, r=0.38 in V1). Moreover, we also find that pairs of boutons with overlapping RFs also tend to show different degrees of tuning similarity (**Figure 14)**. Despite these drawbacks the fact that we find a significant trend suggests that local tuning biases in thalamocortical inputs to mouse V1 may indeed exist.

Similar to our findings, two recent studies of the mouse SC demonstrate that cells representing the same region of visual space have the same preference towards motion along a specific axis [55,110]. These findings, together with our results, suggest that local tuning biases in the thalamocortical network originate from the biases in the local arrangement of retinal ganglion cells [102].

METHODS

Animals

All procedures were approved by the University of California, Los Angeles, Office of Animal Research Oversight (the Institutional Animal Care and Use Committee) and were in accord with guidelines set by the US National Institutes of Health. A total of three C57BL/6J mice (The Jackson Laboratory), were used in this study. Mice were housed in groups of 2 or 3, in reversed light cycle. Animals were naïve subjects with no prior history of participation in research studies. We imaged **[9]** different fields to obtain the data discussed in this paper.

Surgery

Carprofen and buprenorphine analgesia were administered preoperatively. Mice were then anesthetized with isoflurane (4–5% induction; 1.5–2% surgery). Core body temperature was maintained at 37.5°C using a feedback heating system. Eyes were coated with a thin layer of ophthalmic ointment to prevent desiccation. Anesthetized mice were mounted in a stereotaxic apparatus. Blunt ear bars were placed in the external auditory meatus to immobilize the head. A portion of the scalp overlying the two hemispheres of the cortex (~8 x 6 mm) was then removed to expose the underlying skull. After the skull was exposed, it was dried and covered by a thin layer of Vetbond. After the Vetbond dried (~15 min), it provided a stable and solid surface to affix the aluminum bracket with dental acrylic. The bracket was then affixed to the skull, and the margins were sealed with Vetbond and dental acrylic to prevent infections.

Virus Injection

We followed a similar procedure for virus injection to express GcaMP6f in LGN axons described elsewhere [54,118] . A 3-mm-diameter region of skull overlying the occipital cortex was removed. Care was taken to leave the dura intact. GcaMP6-slow was expressed in the dorsal lateral geniculate nucleus (dLGN) using adeno-associated virus. AAV-GcaMP6-slow was loaded into a glass micropipette and slowly inserted into the dLGN using a micromanipulator. AAV-GcaMP6-slow was pressure-injected using a Picospritzer. The injections were made by a computer program in control of the micromanipulator and the Picospritzer.

A sterile 3-mm-diameter cover glass was then placed directly on the dura and sealed at its edges with Vetbond. When dry, the edges of the cover glass were further sealed with dental acrylic. At the end of the surgery, all exposed skull and wound margins were sealed with Vetbond and dental acrylic, and a small, sealed glass window was left in place over the occipital cortex. The mouse was then removed from the stereotaxic apparatus, given a subcutaneous bolus of warm sterile saline, and allowed to recover on the heating pad. When fully alert, it was placed back in its home cage.

Imaging

Once expression of GcaMP was observed in thalamic boutons within the layers of primary visual cortex, typically between 2 to 3 weeks after the injection, imaging sessions took place. Imaging was performed using a resonant, two-photon microscope (Neurolabware, Los Angeles, CA) controlled by Scanbox acquisition software (Los Angeles, CA). The light source was a Coherent Chameleon Ultra II laser (Santa Clara, CA) running at 920 nm. The objective was a □16 water immersion lens (0.8 numerical aperture, 3-mm working distance; Nikon). The microscope frame rate was 15.6 Hz (512 lines with a resonant mirror at 8 kHz). Eye movements and pupil size were recorded via a Dalsa Genie M1280 camera (Teledyne Dalsa) fitted with a 740-nm long-pass filter that looked at the eye indirectly through the reflection of an infrared- reflecting glass.

Visual stimulation

Sequences of pseudorandom sinusoidal gratings [119,120] and checkered bars were generated in real-time by a Processing sketch using OpenGL shaders (see https://processing.org) on a wide screen spanning 100 x 55 in degrees and refreshed at 60 Hz.

In generating pseudo-random gratings, the orientation domain was sampled in equal steps of 10° for a total of 18 possible orientations; the spatial frequency domain was sampled in equal steps on a logarithmic scale from 0.0079 to 0.1549 cycles/°, for a total of 12 possible spatial frequencies; and for each combination of orientation and spatial frequency, spatial phase was equally sampled in steps of 45°, leading to a total of 8 possible settings. The tuning kernels (see *Kernel Estimation*) were computed by averaging responses over spatial phase, as done in previous studies (Malone and Ringach 2008; Ringach et al. 2002). The duration of the sequences was 20 min, and gratings were updated 4 times a second.

To estimate the locations of the receptive fields an elongated bar, composed of a flickering checkerboard pattern, was briefly presented at a random location and orientation on the screen. Bar were replaced with a different bar with a random position and angle 4 times per second. The bars always spanned the entire screen and were 10 degrees wide. The total duration of the stimulus was 25 minutes.

Transistor-transistor logic signals generated by the stimulus computer were sampled by the microscope and time-stamped with the frame and line number being scanned at that time. The timestamps provided the synchronization between visual stimulation and imaging data.

In all experiments, we used a Samsung CHG90 monitor viewed at 20-cm distance. The screen was calibrated using a Photo Research (Chatsworth, CA) PR-650 spectroradiometer, and the result was used to generate the appropriate -corrections for the red, green, and blue components via an NVIDIA Quadro K4000 graphics card. The contrast of the stimulus was 80%. The center of the monitor was positioned with the center of the receptive field population for the eye

contralateral to the cortical hemisphere under consideration. We imaged the monocular region of V1 in the left hemisphere.

Image processing

The image processing pipeline was the similar to that described in detail elsewhere [93] . Briefly, calcium images were aligned to correct for motion artifacts. Following motion stabilization, we used a MATLAB (MathWorks, Natick, MA) graphical user interface tool developed in our laboratory to define regions of interest manually. These regions corresponded micrometer-sized circular or elliptical boutons of dLGN axons. Following segmentation, we extracted signals by computing the mean of the calcium fluorescence within each region of interest and discounting the signals from the nearby neuropil. Spikes were then estimated via deconvolution [121]

Estimation of Kernels

The estimation of a tuning kernel was performed by fitting a linear model between the inferred spiking response of a bouton and the grating stimulus at multiple time lags [93] (Jimenez 2018). Similarly, we computed the retinotopic map of a bouton by fitting a time lagged linear model between the response and the location of bars.

We used bouton kernels at their optimal time delay between the stimulus and response. The optimal delay for a tuning kernel was defined as the time at which the variance of the kernel reached its maximum. A tuning kernel was defined as significant if the peak variance was at least 1.75 times that of the baseline measured at negative time lags.

We defined the optimal delay time for the retinotopic map as the one at which the map's kurtosis reached its maximum. RF maps were deemed significant if their kurtosis value exceeded a value of 13. This kurtosis threshold assured that only RFs highly localized peaks were included. These optimal retinotopic map were then smoothed with the Gaussian window of 5 degrees of visual space. The results presented here use data from boutons with significant tuning kernels and significant retinotopic maps.

We denote the estimated tuning kernel and retinotopic kernel of the i-th bouton in an imaging field by H_T^i and H_{RF}^i, respectively.

Estimation of orientation and spatial frequency preference

We also denote the preferred spatial frequency of the ith bouton as ω^i, defined as the center of mass of the horizontal slice of the tuning kernel passing through the peak response (**Figure 1**). Similarly, we denote the preferred orientation of each bouton as θ^i, defined as the center of mass of the vertical slice of the tuning kernel passing through the peak response (**Figure 1**).

Tuning similarity and RF overlap

We defined joint tuning similarity of bouton pairs as the correlation coefficient between their joint tuning kernels.

$$d_T^{ij} = \frac{\langle H_T^i, H_T^j \rangle}{\|H_T^i\| \|H_T^j\|}$$

We defined the overlap of the receptive fields of pairs of boutons as the correlation coefficient between their receptive field maps.

$$d_{RF}^{jk} = \frac{\langle H_{RF}^{i}, H_{RF}^{j} \rangle}{\|H_{RF}^{i}\| \|H_{RF}^{j}\|}$$

For Wilcoxin rank-sum tests, we assessed tuning similarity for boutons with RFs showing high overlap and those with low overlap. Bouton pairs were deemed to have high RF overlap if the correlation between their RFs fell within the upper quartile of the population RF correlation distribution. Boutons were deemed to low RFs overlap if their correlations fell in the lower quartile of the population RF distribution.

CONCLUSION

ALTERNATIVE MODELS

The limited input model assessed here is part of a broader family of models inspired by the work of Hubel and Wiesel [50]. These models assert that untuned, spatially neighboring ON and OFF signals converge onto a common cortical target endowing it with orientation tuning. Comparing the predictions of the limited input model with physiological data from the mouse is needed to assess how far the mammalian visual system diverges from a purely 'feedforward' information processing system. A variety of other models exist, some of which can supplement the limited input model and help account for some of the tuning properties of simple cells that it fails to explain.

INHERITANCE MODELS OF CORTICAL ORIENTATION TUNING

Ample evidence points to the notion that orientation tuning of mouse V1 neurons is partially determined by their already selective thalamic inputs [56]. The mouse dLGN contains orientation tuned cells [33,34,45,47,48,51,56], particularly, those in the shell region which send axons the superficial layers V1 [39]. Tuned dLGN boutons from the core also innervate multiple V1 layers [54]. Moreover, tuned dLGN neurons [9,33,34,45,48,53] and their axonal projections to V1 [39,54] show a biased preferences towards cardinal orientations, which has sometimes been observed V1 cells [54,68]. Further evidence is that the sharpness orientation selectivity of dLGN neurons is similar to the selectivity of the subthreshold response of cortical cells [56,91]. These findings are consistent with the idea that V1 directly inherit its orientation selectivity from the dLGN (**Figure 15**).

INTRACORTICAL MODELS OF CORTICAL TUNING

Models that invoke broad or null-orientation tuned inhibitory synaptic inputs have also proposed to explain tuning properties of V1 simple cells that feedforward models are unable to account for, such as the increased sharpness of the spiking output, cross orientation suppression and contrast invariance tuning [67,100] . Indeed, inhibitory mechanisms have already been properted to shape tuning in mouse dLGN[48]. Intracortical inhibitory mechanisms are also likely to shape tuning in mouse V1 given that inhibitory interneurons make up ~30% of the V1 population [60,86]. Furthermore, L2/3 cells are innervated by the axons of inhibitory neurons most of which originate from within L2/3[69,70]. Most classes of V1 inhibitory neurons are poorly selective to stimulus orientation [81,122] (although see [85]), have large RFs, and have overlapping subregions [81,83,85]. Therefore, similar mechanism involving broadly tuned recurrent inhibition may also contribute orientation tuning of simple cells.

Orientation selectivity can be further shaped via wiring of excitatory neurons with similar orientation preferences [72-74]. The subthreshold response of a V1 neuron to non-preferred orientations could theoretically be reduced by excitatory inputs originating from other V1 cells with similar preferences, which produce little no spikes in response to null orientations [67,81] . However, this mechanism is debatable to exist in mice, where V1 neurons only *tend* to receive

inputs from excitatory cells with similar preferences, meaning that they also receive some broadly tuned input as well [60,74]. Finally, non-linear spike thresholding may also serve to filter out weaker subthreshold depolarizations evoked by non-preferred orientations [123].

In summary, recurrent inhibitory or excitatory factors, or intracellular non-linearities should also shape the tuning properties of simple cells in mouse V1.

Limited Input Model Vs. Formation Models

The models of tuning discussed up to this point offers a description of the visual system in a steady state where simple cells already exhibit orientation selective responses. However, another question is how simple cells *develop* a highly structured RF with ON and OFF subregions that endow cells with their orientaiton tuning [97]. Developmental models have been proposed to answer these question, however, they tend to invoke specific learning rules or developmental processes.

The limited input model offers a simpler solution to this problem by making a simple set of evidence based assumptions regarding the spatial layout of ON/OFF RGCs and the size of the retinal pool available to a post synaptic cell. Namely, the model asserts that retinal regions are *sparsely* covered by ON and OFF center surround cells which naturally arrange themeselves into dipoles (**Figure 9**). Moreover, the model *rejects* the idea that a postsynaptic cell samples signals from a large number of inputs, and instead posits that only a small, spatially compact pool of RGCs inputs are availabe for the cell[117].

Given these assumptions, the model parsimounously explains how cells aquire their tuning. Consider for example, a post synaptic neurons that pools inputs from a limited number of neighboring RGCs that sparsely cover a local retinal region. Such a neuron can simply pool inputs, *at random*, and it would have a good chance of selecting signals that are spatially displaced, endowing it with spatially offset subregions and consequentially, orientation tuning Also consider the implication of forcing a neuron to pool from a small compact region of retina tiled by ON-OFF RGC dipoles. Again, pooling inputs at random from a small region would endow the post synaptic neuron cell with side-by-side ON-OFF subregions and orientation selectivity. Indeed, merely restricting the number of inputs or the spatial extent of the retinal input pool will help a post synaptic neurons develop selectivity: Limiting the inputs would constrain the number of spatial arrangements that retinal RFs can form, most notably, ‘inappropriate’ arrangements. In other words, limiting inputs safe guards the post synaptic cell from building an innapropriate RF that would preclude orientation tuning[117]. Thus the limited input model explains the emergence of orientation tuning all while assuming that post synaptic neurons pooled their inputs at *random*. In this sense, the model is parsimonous.

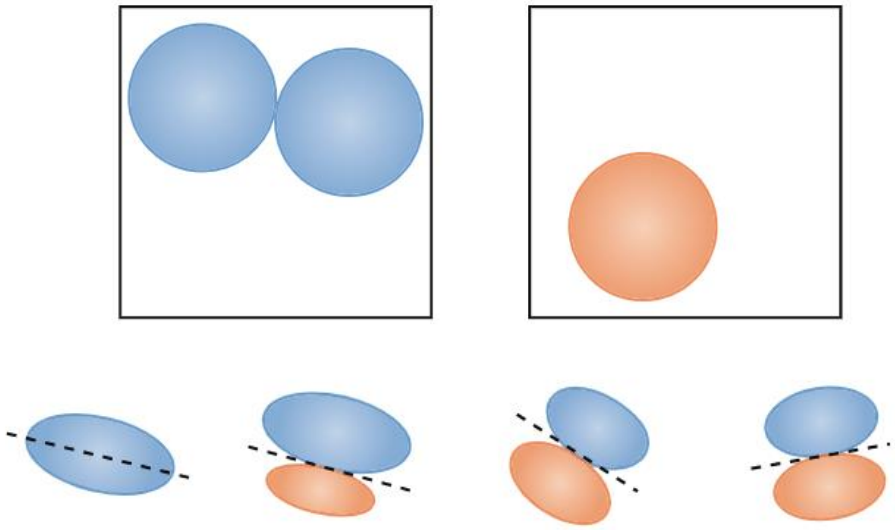

FIGURE 16 LIMITING THE NUMBER OF AVAILABLE INPUTS LIMITS THE TYPES OF RFS A POST SYNAPTIC NEURON CAN BUILD

In the limited-input model, only a handful of receptive fields can be combined to generate a receptive field. As shown on the bottom, only a limited range of orientations (clustering near the horizontal) can be produced with the given resources on the left. Cells that randomly select inputs from such a limited input pool are likely to select an 'appropriately' arranged set of center surround retinal inputs.
Figure taken directly from Ringach 2011.

NORMATIVE APPROACHES

There is alternative approach to the study tuning, which aims to answer *why* it exists, with less emphasis on accurately describing the physical process that generates tuning. That is, one could ask what is the *function* of tuning of single cells, the specific wiring schemes or pooling methods used by neurons to select their inputs or project their signals, or anatomical organizations of tuned cells.

THE FUNCTION OF SINGLE CELL TUNING

For example, has been proposed that the purpose of having visual cells tuned to specific image features is to summarize the vast amount of information that bombards the sensory surface [124] , a necessary step for storage and commutations purposes [125] . In order to maximize the number of relevant image features that can be encoded, simple cells are tuned to contrast polarity, which simultaneously provides sensitivity to the polar contrast of a stimulus as well as its orientation.

Perhaps most obvious benefit of neuronal orientation tuning is that it is necessary to extract shape information which in turn is needed to reconstruct the sensory image [126] .

The function of Wiring

Randomly wiring neurons together, as opposed to using specific wiring patterns, may simplify the rules the visual system uses to build itself. Moreover, the purpose of retinothalamic or thalamocortical convergence is said to increase the capacity of the brain to enhance the spatially resolution of the visual image [127].

A highly influential theory posits that minimizing the amount of wiring serves many benefits including: reducing metabolic costs; increasing the speed of information transmission; maximizing the number of synapses available to each neuron [128], and increasing the number of features that can be encoded by neurons at each point in visual space [107].

The function of Cortical Maps

The cortex is remarkably uniform [92] and appears be composed of columns of cells with similar functional responses. Using the same column of cells as a basic building block that gets repeated across cortex may simplify the rules used to build the cortex, reduce the number of different types computations that need to be performed on sensory information [129], and may possibly serve as the basis of organized planned behavior [130].

Arranging cells in a retinotopic manner has been proposed to facilitate computations in local image regions [131], which are arguably the most important computations that need to be performed. Furthermore, optimally organizing maps of different stimulus features (e.g., at 90 degrees) across the cortical surface may minimize the occurrence of visual 'scotomas' [132], while exponentially expanding the size of the cortex may increase the number of features encoded at each point in visual space [2].

CLOSING REMARKS

Modeling the emergence of orientation tuning has and continues to have a dramatic impact on our understanding of sensory processing. One should embrace the possibility that tuning emerges according to different mechanisms in different brain structures and in different species each with their own unique behavioral needs. We should also continue to draw inspiration by studying the sensory systems of multiple species with the aim of discovering universal sensory computations.

BIBLIOGRAPHY

1 Breedlove, S. M. & Watson, N. V. *Behavioral neuroscience*. (Sinauer Associates, Incorporated, Publishers, 2018).

2 Kremkow, J. & Alonso, J.-M. Thalamocortical Circuits and Functional Architecture. (2018).

3 Ibbotson, M. & Jung, Y. J. Origins of Functional Organization in the Visual Cortex. *Frontiers in Systems Neuroscience* **14**, 1-13, doi:10.3389/fnsys.2020.00010 (2020).

4 Borst, A. & Helmstaedter, M. Common circuit design in fly and mammalian motion vision. *Nature Neuroscience* **18**, 1067-1076, doi:10.1038/nn.4050 PMID - 26120965 (2015).

5 Masland, R. H. The fundamental plan of the retina. *Nature Neuroscience* **4**, 877-886, doi:10.1038/nn0901-877 PMID - 11528418 (2001).

6 Baden, T. *et al.* The functional diversity of retinal ganglion cells in the mouse. *Nature* **529**, 345-350, doi:10.1038/nature16468 PMID - 26735013 (2016).

7 Bae, J. A. *et al.* Digital Museum of Retinal Ganglion Cells with Dense Anatomy and Physiology. *Cell* **173**, 1293-1306.e1219, doi:10.1016/j.cell.2018.04.040 (2018).

8 Masland, R. H. The Neuronal Organization of the Retina. *Neuron* **76**, 266-280, doi:10.1016/j.neuron.2012.10.002 (2012).

9 Román Rosón, M. *et al.* Mouse dLGN Receives Functional Input from a Diverse Population of Retinal Ganglion Cells with Limited Convergence. *Neuron* **102**, 462-476.e468, doi:10.1016/j.neuron.2019.01.040 (2019).

10 Wässle, H., Boycott, B. B. & Illing, R. b. Morphology and mosaic of on- and off-beta cells in the cat retina and some functional considerations. *Proceedings of the Royal Society of London. Series B. Biological Sciences* **212**, 177-195, doi:10.1098/rspb.1981.0033 PMID - 6166013 (1981).

11 Reese, B. E. Development of the retina and optic pathway. *Vision Research* **51**, 613-632, doi:10.1016/j.visres.2010.07.010 PMID - 20647017 (2011).

12 Gauthier, J. L. *et al.* Uniform Signal Redundancy of Parasol and Midget Ganglion Cells in Primate Retina. *The Journal of Neuroscience* **29**, 4675-4680, doi:10.1523/jneurosci.5294-08.2009 PMID - 19357292 (2009).

13 Bleckert, A., Schwartz, G. W., Turner, M. H., Rieke, F. & Wong, R. O. L. Visual space is represented by nonmatching topographies of distinct mouse retinal ganglion cell types. *Current Biology* **24**, 310-315, doi:10.1016/j.cub.2013.12.020 (2014).

14 Heukamp, A. S., Warwick, R. A. & Rivlin-Etzion, M. Topographic Variations in Retinal Encoding of Visual Space. *Annual Review of Vision Science* **6**, 1-23, doi:10.1146/annurev-vision-121219-081831 (2020).

15 Wei, W. Neural mechanisms of motion processing in the mammalian retina. *Annual Review of Vision Science* **4**, 165-192, doi:10.1146/annurev-vision-091517-034048 (2018).

16 Remtulla, S. a. H. P. E. A schematic eye for the mouse, and comparisons with the rat. *Vision Research* **25**, 21--31, doi:10.1016/0042-6989(85)90076-8 (1985).

17 Rousso, David L. *et al.* Two Pairs of ON and OFF Retinal Ganglion Cells Are Defined by Intersectional Patterns of Transcription Factor Expression. *Cell Reports* **15**, 1930-1944, doi:10.1016/j.celrep.2016.04.069 PMID - 27210758 (2016).

18 Busse, L. Chapter 4 The Mouse Visual System and Visual Perception. *Handbook of Behavioral Neuroscience* **27**, 53–68, doi:10.1016/b978-0-12-812012-5.00004-5 (2018).

19 Krieger, B., Qiao, M., Rousso, D. L., Sanes, J. R. & Meister, M. Four alpha ganglion cell types in mouse retina: Function, structure, and molecular signatures. *PLOS ONE* **12**, e0180091, doi:10.1371/journal.pone.0180091 PMID - 28753612 (2017).

20 Busse, L. The Mouse Visual System and Visual Perception. *Handbook of Behavioral Neuroscience* **27**, 53-68, doi:10.1016/B978-0-12-812012-5.00004-5 (2018).

21 Dhande, O. S., Stafford, B. K., Lim, J.-H. A. & Huberman, A. D. Contributions of Retinal Ganglion Cells to Subcortical Visual Processing and Behaviors. *Annual Review of Vision Science* **1**, 291-328, doi:10.1146/annurev-vision-082114-035502 (2015).

22 Zhang, Y., Kim, I. J., Sanes, J. R. & Meister, M. The most numerous ganglion cell type of the mouse retina is a selective feature detector. *Proceedings of the National Academy of Sciences of the United States of America* **109**, E2391-E2398, doi:10.1073/pnas.1211547109 (2012).

23 Warwick, R. A., Kaushansky, N., Sarid, N., Golan, A. & Rivlin-Etzion, M. Inhomogeneous Encoding of the Visual Field in the Mouse Retina. *Current Biology* **28**, 655-665.e653, doi:10.1016/j.cub.2018.01.016 (2018).

24 Kim, I. J., Zhang, Y., Yamagata, M., Meister, M. & Sanes, J. R. Molecular identification of a retinal cell type that responds to upward motion. *Nature* **452**, 478-482, doi:10.1038/nature06739 (2008).

25 Ekesten, B. & Gouras, P. Cone and rod inputs to murine retinal ganglion cells: Evidence of cone opsin specific channels. *Visual Neuroscience* **22**, 893-903, doi:10.1017/s0952523805226172 PMID - 16469196 (2005).

26 Wang, Y. V., Weick, M. & Demb, J. B. Spectral and Temporal Sensitivity of Cone-Mediated Responses in Mouse Retinal Ganglion Cells. **31**, 7670-7681, doi:10.1523/JNEUROSCI.0629-11.2011 (2011).

27 Chang, L., Breuninger, T. & Euler, T. Chromatic Coding from Cone-type Unselective Circuits in the Mouse Retina. *Neuron* **77**, 559-571, doi:10.1016/j.neuron.2012.12.012 PMID - 23395380 (2013).

28 Szatko, K. P. *et al.* Neural circuits in the mouse retina support color vision in the upper visual field. *Nature Communications* **11**, 3481, doi:10.1038/s41467-020-17113-8 PMID - 32661226 (2020).

29 Martersteck, E. M. *et al.* Diverse Central Projection Patterns of Retinal Ganglion Cells. *Cell Reports* **18**, 2058-2072, doi:10.1016/j.celrep.2017.01.075 (2017).

30 Guido, W. Development, form, and function of the mouse visual thalamus. *Journal of Neurophysiology* **120**, 211-225, doi:10.1152/jn.00651.2017 (2018).

31 Ellis, E. M., Gauvain, G., Sivyer, B. & Murphy, G. J. Shared and distinct retinal input to the mouse superior colliculus and dorsal lateral geniculate nucleus. *Journal of Neurophysiology* **116**, 602-610, doi:10.1152/jn.00227.2016 PMID - 27169509 (2016).

32 Mazade, R. & Alonso, J. M. Thalamocortical processing in vision. *Visual Neuroscience* **34**, E007-E007, doi:10.1017/S0952523817000049 (2017).

33 Liang, L. *et al.* A Fine-Scale Functional Logic to Convergence from Retina to Thalamus. *Cell* **173**, 1343-1355.e1324, doi:10.1016/j.cell.2018.04.041 (2018).

34 Piscopo, D. M., El-Danaf, R. N., Huberman, A. D. & Niell, C. M. Diverse Visual Features Encoded in Mouse Lateral Geniculate Nucleus. *Journal of Neuroscience* **33**, 4642-4656, doi:10.1523/JNEUROSCI.5187-12.2013 (2013).

35 Pfeiffenberger, C. *et al.* Ephrin-As and neural activity are required for eye-specific patterning during retinogeniculate mapping. *Nature Neuroscience* **8**, 1022-1027, doi:10.1038/nn1508 PMID - 16025107 (2005).

36 Hong, Y. K., Burr, E. F., Sanes, J. R. & Chen, C. Heterogeneity of retinogeniculate axon arbors. *European Journal of Neuroscience* **49**, 948-956, doi:10.1111/ejn.13986 PMID - 29883007 (2019).

37 Huberman, A. D. *et al.* Architecture and Activity-Mediated Refinement of Axonal Projections from a Mosaic of Genetically Identified Retinal Ganglion Cells. *Neuron* **59**, 425-438, doi:10.1016/j.neuron.2008.07.018 (2008).

38 Huberman, A. D., Feller, M. B. & Chapman, B. Mechanisms underlying development of visual maps and receptive fields. *Annual Review of Neuroscience* **31**, 479-509, doi:10.1146/annurev.neuro.31.060407.125533 (2008).

39 Cruz-Martín, A. *et al.* A dedicated circuit links direction-selective retinal ganglion cells to the primary visual cortex. *Nature* **507**, 358-361, doi:10.1038/nature12989 PMID - 24572358 (2014).

40 Huberman, A. D. *et al.* Genetic Identification of an On-Off Direction- Selective Retinal Ganglion Cell Subtype Reveals a Layer-Specific Subcortical Map of Posterior Motion. *Neuron* **62**, 327-334, doi:10.1016/j.neuron.2009.04.014 (2009).

41 Kay, J. N. *et al.* Retinal Ganglion Cells with Distinct Directional Preferences Differ in Molecular Identity, Structure, and Central Projections. *The Journal of Neuroscience* **31**, 7753-7762, doi:10.1523/jneurosci.0907-11.2011 PMID - 21613488 (2011).

42 Rivlin-Etzion, M. *et al.* Transgenic Mice Reveal Unexpected Diversity of On-Off Direction-Selective Retinal Ganglion Cell Subtypes and Brain Structures Involved in Motion Processing. *The Journal of Neuroscience* **31**, 8760-8769, doi:10.1523/jneurosci.0564-11.2011 PMID - 21677160 (2011).

43 Kim, I.-J., Zhang, Y., Meister, M. & Sanes, J. R. Laminar Restriction of Retinal Ganglion Cell Dendrites and Axons: Subtype-Specific Developmental Patterns Revealed with Transgenic Markers. *The Journal of Neuroscience* **30**, 1452-1462, doi:10.1523/jneurosci.4779-09.2010 PMID - 20107072 (2010).

44 Howarth, M., Walmsley, L. & Brown, Timothy M. Binocular Integration in the Mouse Lateral Geniculate Nuclei. *Current Biology* **24**, 1241-1247, doi:10.1016/j.cub.2014.04.014 PMID - 24856206 (2014).

45 Zhao, X., Chen, H., Liu, X. & Cang, J. Orientation-selective Responses in the Mouse Lateral Geniculate Nucleus. **33**, 12751-12763, doi:10.1523/JNEUROSCI.0095-13.2013 (2013).

46 Tang, J., Jimenez, S. C. A., Chakraborty, S. & Schultz, S. R. Visual receptive field properties of neurons in the mouse lateral geniculate nucleus. *PLoS ONE* **11**, 1-34, doi:10.1371/journal.pone.0146017 (2016).

47 Grubb, M. S. & Thompson, I. D. Quantitative Characterization of Visual Response Properties in the Mouse Dorsal Lateral Geniculate Nucleus. *Journal of Neurophysiology* **90**, 3594-3607, doi:10.1152/jn.00699.2003 (2003).

48 Suresh, V. *et al.* Synaptic contributions to receptive field structure and response properties in the rodent lateral geniculate nucleus of the thalamus. *Journal of Neuroscience* **36**, 10949-10963, doi:10.1523/JNEUROSCI.1045-16.2016 (2016).

49 Lien, A. D. & Scanziani, M. Cortical direction selectivity emerges at convergence of thalamic synapses. *Nature* **558**, 80-86, doi:10.1038/s41586-018-0148-5 PMID - 29795349 (2018).

50 Hubel, D. H. & Wiesel, T. N. Receptive fields, binocular interaction and functional architecture in the cat's visual cortex. *The Journal of Physiology* **160**, 106-154, doi:10.1113/jphysiol.1962.sp006837 PMID - 14449617 (1962).

51 Vidyasagar, T. R. & Eysel, U. T. Origins of feature selectivities and maps in the mammalian primary visual cortex. *Trends in Neurosciences* **38**, 475-485, doi:10.1016/j.tins.2015.06.003 (2015).

52 Marshel, J. H., Garrett, M. E., Nauhaus, I. & Callaway, E. M. Functional specialization of seven mouse visual cortical areas. *Neuron* **72**, 1040-1054, doi:10.1016/j.neuron.2011.12.004 (2011).

53 Marshel, J. H., Kaye, A. P., Nauhaus, I. & Callaway, E. M. Anterior-Posterior Direction Opponency in the Superficial Mouse Lateral Geniculate Nucleus. *Neuron* **76**, 713-720, doi:10.1016/j.neuron.2012.09.021 (2012).

54 Sun, W., Tan, Z., Mensh, B. D. & Ji, N. Thalamus provides layer 4 of primary visual cortex with orientation- and direction-tuned inputs. *Nature Neuroscience* **19**, 308-315, doi:10.1038/nn.4196 PMID - 26691829 (2016).

55 Ahmadlou, M. & Heimel, J. A. Preference for concentric orientations in the mouse superior colliculus. *Nature Communications* **6**, 6773, doi:10.1038/ncomms7773 PMID - 25832803 (2015).

56 Scholl, B., Tan, A. Y. Y., Corey, J. & Priebe, N. J. Emergence of Orientation Selectivity in the Mammalian Visual Pathway. *The Journal of Neuroscience* **33**, 10616-10624, doi:10.1523/jneurosci.0404-13.2013 PMID - 23804085 (2013).

57 Hammer, S., Monavarfeshani, A., Lemon, T., Su, J. & Fox, M. A. Multiple Retinal Axons Converge onto Relay Cells in the Adult Mouse Thalamus. *Cell Reports* **12**, 1575-1583, doi:10.1016/j.celrep.2015.08.003 (2015).

58 Rompani, S. B. *et al.* Different Modes of Visual Integration in the Lateral Geniculate Nucleus Revealed by Single-Cell-Initiated Transsynaptic Tracing. *Neuron* **93**, 767-776.e766, doi:10.1016/j.neuron.2017.01.028 PMID - 28231464 (2017).

59 Froudarakis, E. *et al.* The Visual Cortex in Context. *Annual Review of Vision Science* **5**, 317-339, doi:10.1146/annurev-vision-091517-034407 (2019).

60 Harris, K. D. & Mrsic-Flogel, T. D. Cortical connectivity and sensory coding. *Nature* **503**, 51-58, doi:10.1038/nature12654 PMID - 24201278 (2013).

61 Ji, X. Y. *et al.* Thalamocortical Innervation Pattern in Mouse Auditory and Visual Cortex: Laminar and Cell-Type Specificity. *Cerebral Cortex* **26**, 2612-2625, doi:10.1093/cercor/bhv099 (2016).

62 Morgenstern, N. A., Bourg, J. & Petreanu, L. Multilaminar networks of cortical neurons integrate common inputs from sensory thalamus. *Nature Neuroscience* **19**, 1034-1040, doi:10.1038/nn.4339 PMID - 27376765 (2016).

63 Ji, W. *et al.* Modularity in the Organization of Mouse Primary Visual Cortex. *Neuron* **87**, 632-643, doi:10.1016/j.neuron.2015.07.004 (2015).

64 Li, Y. T., Ibrahim, L. A., Liu, B. H., Zhang, L. I. & Tao, H. W. Linear transformation of thalamocortical input by intracortical excitation. *Nature Neuroscience* **16**, 1324-1330, doi:10.1038/nn.3494 (2013).

65 Lien, A. D. & Scanziani, M. Tuned thalamic excitation is amplified by visual cortical circuits. *Nature Neuroscience* **16**, 1315-1323, doi:10.1038/nn.3488 PMID - 23933748 (2013).

66 Chung, S. & Ferster, D. Strength and Orientation Tuning of the Thalamic Input to Simple Cells Revealed by Electrically Evoked Cortical Suppression. *Neuron* **20**, 1177-1189, doi:10.1016/s0896-6273(00)80498-5 PMID - 9655505 (1998).

67 Finn, I. M., Priebe, N. J. & Ferster, D. The Emergence of Contrast-Invariant Orientation Tuning in Simple Cells of Cat Visual Cortex. *Neuron* **54**, 137-152, doi:10.1016/j.neuron.2007.02.029 PMID - 17408583 (2007).

68 Ohtsuki, G. *et al.* Similarity of visual selectivity among clonally related neurons in visual cortex. *Neuron* **75**, 65-72, doi:10.1016/j.neuron.2012.05.023 (2012).

69 Wertz, A. *et al.* Single-cell–initiated monosynaptic tracing reveals layer-specific cortical network modules. *Science* **349**, 70-74, doi:10.1126/science.aab1687 PMID - 26138975 (2015).

70 Rossi, L. F., Harris, K. D. & Carandini, M. Spatial connectivity matches direction selectivity in visual cortex. *Nature* **588**, 1-5, doi:10.1038/s41586-020-2894-4 PMID - 33177719 (2020).

71 Yoshimura, Y. & Callaway, E. M. Fine-scale specificity of cortical networks depends on inhibitory cell type and connectivity. *Nature Neuroscience* **8**, 1552-1559, doi:10.1038/nn1565 PMID - 16222228 (2005).

72 Ko, H. *et al.* Functional specificity of local synaptic connections in neocortical networks. *Nature* **473**, 87-91, doi:10.1038/nature09880 (2011).

73 Ko, H. *et al.* The emergence of functional microcircuits in visual cortex. *Nature* **496**, 96-100, doi:10.1038/nature12015 (2013).

74 Cossell, L. *et al.* Functional organization of excitatory synaptic strength in primary visual cortex. *Nature* **518**, 399-403, doi:10.1038/nature14182 PMID - 25652823 (2015).

75 Gilbert, C. D. & Wiesel, T. N. Columnar specificity of intrinsic horizontal and corticocortical connections in cat visual cortex. *Journal of Neuroscience* **9**, 2432-2442, doi:10.1523/jneurosci.09-07-02432.1989 PMID - 2746337 (1989).

76 Malach, R., Amir, Y., Harel, M. & Grinvald, A. Relationship between intrinsic connections and functional architecture revealed by optical imaging and in vivo targeted biocytin injections in primate striate cortex. *Proceedings of the National Academy of Sciences* **90**, 10469-10473, doi:10.1073/pnas.90.22.10469 PMID - 8248133 (1993).

77 Bosking, W. H., Zhang, Y., Schofield, B. & Fitzpatrick, D. Orientation Selectivity and the Arrangement of Horizontal Connections in Tree Shrew Striate Cortex. *Journal of Neuroscience* **17**, 2112-2127, doi:10.1523/jneurosci.17-06-02112.1997 PMID - 9045738 (1997).

78 Yu, Y. C., Bultje, R. S., Wang, X. & Shi, S. H. Specific synapses develop preferentially among sister excitatory neurons in the neocortex. *Nature* **458**, 501-504, doi:10.1038/nature07722 (2009).

79 Li, Y. *et al.* Clonally related visual cortical neurons show similar stimulus feature selectivity. *Nature* **486**, 118-121, doi:10.1038/nature11110 (2012).

80 Yu, Y. C. *et al.* Preferential electrical coupling regulates neocortical lineage-dependent microcircuit assembly. *Nature* **486**, 113-117, doi:10.1038/nature10958 (2012).

81 Niell, C. M. & Stryker, M. P. Highly Selective Receptive Fields in Mouse Visual Cortex. *The Journal of Neuroscience* **28**, 7520-7536, doi:10.1523/jneurosci.0623-08.2008 PMID - 18650330 (2008).

82 Smith, S. L. & Häusser, M. Parallel processing of visual space by neighboring neurons in mouse visual cortex. *Nature Neuroscience* **13**, 1144-1149, doi:10.1038/nn.2620 (2010).

83 Liu, B. H. *et al.* Visual receptive field structure of cortical inhibitory neurons revealed by two-photon imaging guided recording. *Journal of Neuroscience* **29**, 10520-10532, doi:10.1523/JNEUROSCI.1915-09.2009 (2009).

84 Liu, B. H. *et al.* Intervening inhibition underlies simple-cell receptive field structure in visual cortex. *Nature Neuroscience* **13**, 89-96, doi:10.1038/nn.2443 (2010).

85 Ma, W. P. *et al.* Visual representations by cortical somatostatin inhibitory neurons - Selective but with weak and delayed responses. *Journal of Neuroscience* **30**, 14371-14379, doi:10.1523/JNEUROSCI.3248-10.2010 (2010).

86 Bonin, V., Histed, M. H., Yurgenson, S. & Reid, R. C. Local diversity and fine-scale organization of receptive fields in mouse visual cortex. *Journal of Neuroscience* **31**, 18506-18521, doi:10.1523/JNEUROSCI.2974-11.2011 (2011).

87 Vaiceliunaite, A., Erisken, S., Franzen, F., Katzner, S. & Busse, L. Spatial integration in mouse primary visual cortex. *Journal of Neurophysiology* **110**, 964-972, doi:10.1152/jn.00138.2013 (2013).

88 Ringach, D. L. Spatial Structure and Symmetry of Simple-Cell Receptive Fields in Macaque Primary Visual Cortex. *Journal of Neurophysiology* **88**, 455-463, doi:10.1152/jn.2002.88.1.455 PMID - 12091567 (2002).

89 Van Hooser, S. D. Similarity and Diversity in Visual Cortex: Is There a Unifying Theory of Cortical Computation? *The Neuroscientist* **13**, 639-656, doi:10.1177/1073858407306597 (2007).

90 Rochefort, N. L. *et al.* Development of direction selectivity in mouse cortical neurons. *Neuron* **71**, 425-432, doi:10.1016/j.neuron.2011.06.013 (2011).

91 Tan, A. Y. Y., Brown, B. D., Scholl, B., Mohanty, D. & Priebe, N. J. Orientation selectivity of synaptic input to neurons in mouse and cat primary visual cortex. *Journal of Neuroscience* **31**, 12339-12350, doi:10.1523/JNEUROSCI.2039-11.2011 (2011).

92 Hubel, D. H. & Wiesel, T. N. Ferrier lecture - Functional architecture of macaque monkey visual cortex. *Proceedings of the Royal Society of London. Series B. Biological Sciences* **198**, 1-59, doi:10.1098/rspb.1977.0085 PMID - 20635 (1977).

93 Ringach, D. L. *et al.* Spatial clustering of tuning in mouse primary visual cortex. *Nature communications* **7**, 12270-12270, doi:10.1038/ncomms12270 (2016).

94 Ohki, K., Chung, S., Ch'ng, Y. H., Kara, P. & Reid, R. C. Functional imaging with cellular resolution reveals precise micro-architecture in visual cortex. *Nature* **433**, 597-603, doi:10.1038/nature03274 (2005).

95 Kremkow, J., Jin, J., Wang, Y. & Alonso, J. M. Principles underlying sensory map topography in primary visual cortex. *Nature* **533**, 52-57, doi:10.1038/nature17936 (2016).

96 Yeh, C.-I., Xing, D., Williams, P. E. & Shapley, R. M. Stimulus ensemble and cortical layer determine V1 spatial receptive fields. *Proceedings of the National Academy of Sciences* **106**, 14652-14657, doi:10.1073/pnas.0907406106 PMID - 19706551 (2009).

97 Jin, J., Wang, Y., Swadlow, H. A. & Alonso, J. M. Population receptive fields of ON and OFF thalamic inputs to an orientation column in visual cortex. *Nature Neuroscience* **14**, 232-238, doi:10.1038/nn.2729 PMID - 21217765 (2011).

98 Chapman, B., Zahs, K. R. & Stryker, M. P. Relation of cortical cell orientation selectivity to alignment of receptive fields of the geniculocortical afferents that arborize within a single orientation column in ferret visual cortex. *Journal of Neuroscience* **11**, 1347-1358, doi:10.1523/jneurosci.11-05-01347.1991 PMID - 2027051 (1991).

99 Lee, K.-S., Huang, X. & Fitzpatrick, D. Topology of ON and OFF inputs in visual cortex enables an invariant columnar architecture. *Nature* **533**, 90-94, doi:10.1038/nature17941 (2016).

100 Priebe, N. J. Mechanisms of Orientation Selectivity in the Primary Visual Cortex. *Annual review of vision science* **2**, 85-107, doi:10.1146/annurev-vision-111815-114456 (2016).

101 Ringach, D. L. Haphazard wiring of simple receptive fields and orientation columns in visual cortex. *Journal of neurophysiology* **92**, 468-476, doi:10.1152/jn.01202.2003 (2004).

102 Paik, S. B. & Ringach, D. L. Retinal origin of orientation maps in visual cortex. *Nature Neuroscience* **14**, 919-925, doi:10.1038/nn.2824 (2011).

103 Ringach, D. L. On the origin of the functional architecture of the cortex. *PLoS ONE* **2**, doi:10.1371/journal.pone.0000251 (2007).

104 Jang, J., Song, M. & Paik, S. B. Retino-Cortical Mapping Ratio Predicts Columnar and Salt-and-Pepper Organization in Mammalian Visual Cortex. *Cell Reports* **30**, 3270-3279.e3273, doi:10.1016/j.celrep.2020.02.038 (2020).

105 Yeh, C. I., Xing, D. & Shapley, R. M. "Black" Responses Dominate Macaque Primary Visual Cortex V1. *Journal of Neuroscience* **29**, 11753-11760, doi:10.1523/JNEUROSCI.1991-09.2009 (2009).

106 Daugman, J. G. Uncertainty relation for resolution in space, spatial frequency, and orientation optimized by two-dimensional visual cortical filters. *Journal of the Optical Society of America A* **2**, 1160, doi:10.1364/josaa.2.001160 PMID - 4020513 (1985).

107 Swindale, N. V., Shoham, D., Grinvald, A., Bonhoeffer, T. & Hübener, M. Visual cortex maps are optimized for uniform coverage. *Nature Neuroscience* **3**, 822-826, doi:10.1038/77731 PMID - 10903576 (2000).

108 Paik, S. B. & Ringach, D. L. Link between orientation and retinotopic maps in primary visual cortex. *Proceedings of the National Academy of Sciences of the United States of America* **109**, 7091-7096, doi:10.1073/pnas.1118926109 (2012).

109 Jimenez, L. O., Tring, E., Trachtenberg, J. T. & Ringach, D. L. Local tuning biases in mouse primary visual cortex. *Journal of Neurophysiology* **120**, 274-280, doi:10.1152/jn.00150.2018 PMID - 29668380 (2018).

110 Feinberg, E. H. & Meister, M. Orientation columns in the mouse superior colliculus. *Nature* **519**, 229-232, doi:10.1038/nature14103 PMID - 25517100 (2015).

111 Ringach, D. in *The New VisualNeurosciences, MA:, 2013.* (eds JS Werner & LM Chalupa) (MIT Press, 2013).

112 Liang, L. *et al.* Retinal Inputs to the Thalamus Are Selectively Gated by Arousal. *Current Biology* **30**, 3923-3934.e3929, doi:10.1016/j.cub.2020.07.065 (2020).

113 Hillier, D. *et al.* Causal evidence for retina-dependent and -independent visual motion computations in mouse cortex. *Nature Neuroscience* **20**, 960-968, doi:10.1038/nn.4566 PMID - 28530661 (2017).

114 Heeger, D. J., Boynton, G. M., Demb, J. B., Seidemann, E. & Newsome, W. T. Motion Opponency in Visual Cortex. *Journal of Neuroscience* **19**, 7162-7174, doi:10.1523/jneurosci.19-16-07162.1999 PMID - 10436069 (1999).

115 Mauss, A. S., Vlasits, A., Borst, A. & Feller, M. Visual Circuits for Direction Selectivity. *Annual Review of Neuroscience* **40**, 1-20, doi:10.1146/annurev-neuro-072116-031335 PMID - 28418757 (2016).

116 Borst, A. & Euler, T. Seeing Things in Motion: Models, Circuits, and Mechanisms. *Neuron* **71**, 974-994, doi:10.1016/j.neuron.2011.08.031 PMID - 21943597 (2011).

117 Ringach, D. L. You get what you get and you don't get upset. *Nature neuroscience* **14**, 123-124, doi:10.1038/nn0211-123 (2011).

118 Kondo, S. & Ohki, K. Laminar differences in the orientation selectivity of geniculate afferents in mouse primary visual cortex. *Nature Neuroscience* **19**, 316-319, doi:10.1038/nn.4215 PMID - 26691830 (2016).

119 Malone, B. J. & Ringach, D. L. Dynamics of Tuning in the Fourier Domain. *Journal of Neurophysiology* **100**, 239-248, doi:10.1152/jn.90273.2008 PMID - 18480369 (2008).

120 Ringach, D. L., Sapiro, G. & Shapley, R. A subspace reverse-correlation technique for the study of visual neurons. *Vision Research* **37**, 2455-2464, doi:10.1016/S0042-6989(96)00247-7 (1997).

121 Berens, P. *et al.* Community-based benchmarking improves spike rate inference from two-photon calcium imaging data. *PLOS Computational Biology* **14**, e1006157, doi:10.1371/journal.pcbi.1006157 PMID - 29782491 (2018).

122 Kerlin, A. M., Andermann, M. L., Berezovskii, V. K. & Reid, R. C. Broadly Tuned Response Properties of Diverse Inhibitory Neuron Subtypes in Mouse Visual Cortex. *Neuron* **67**, 858-871, doi:10.1016/j.neuron.2010.08.002 PMID - 20826316 (2010).

123 Priebe, N. J. & Ferster, D. Inhibition, Spike Threshold, and Stimulus Selectivity in Primary Visual Cortex. *Neuron* **57**, 482-497, doi:10.1016/j.neuron.2008.02.005 (2008).

124 Pang, R., Lansdell, B. J. & Fairhall, A. L. Dimensionality reduction in neuroscience. *Current Biology* **26**, R656-R660, doi:10.1016/j.cub.2016.05.029 PMID - 27458907 (2016).

125 Daugman, J. G. Complete Discrete 2-D Gabor Transforms by Neural Networks for Image Analysis and Compression. *IEEE Transactions on Acoustics, Speech, and Signal Processing* **36**, 1169-1179, doi:10.1109/29.1644 (1988).

126 Hoffman, D. D. & Richards, W. A. Parts of recognition. *Cognition* **18**, 65-96, doi:10.1016/0010-0277(84)90022-2 PMID - 6543164 (1984).

127 Martinez, Luis M., Molano-Mazón, M., Wang, X., Sommer, Friedrich T. & Hirsch, Judith A. Statistical Wiring of Thalamic Receptive Fields Optimizes Spatial Sampling of the Retinal Image. *Neuron* **81**, 943-956, doi:10.1016/j.neuron.2013.12.014 PMID - 24559681 (2014).

128 Chklovskii, D. B., Schikorski, T. & Stevens, C. F. Wiring Optimization in Cortical Circuits. *Neuron* **34**, 341-347, doi:10.1016/s0896-6273(02)00679-7 PMID - 11988166 (2002).

129 Hubel, D. H. & Wiesel, T. N. Brain mechanisms of vision. *Scientific American* **241**, 150-163 (1979).

130 Swindale. Visual Cortex: More Wiggle Room for the Brain. *Current Biology*, doi:10.1016/j.cub.2007.10.032 (2007).

131 Cowey, A. Cortical maps and visual perception: the Grindley Memorial Lecture. *The Quarterly journal of experimental psychology* **31**, 1-17, doi:10.1080/14640747908400703 (1979).

132 Swindale, N. V. Coverage and the design of striate cortex. *Biological Cybernetics* **65**, 415-424, doi:10.1007/bf00204654 PMID - 1958727 (1991).